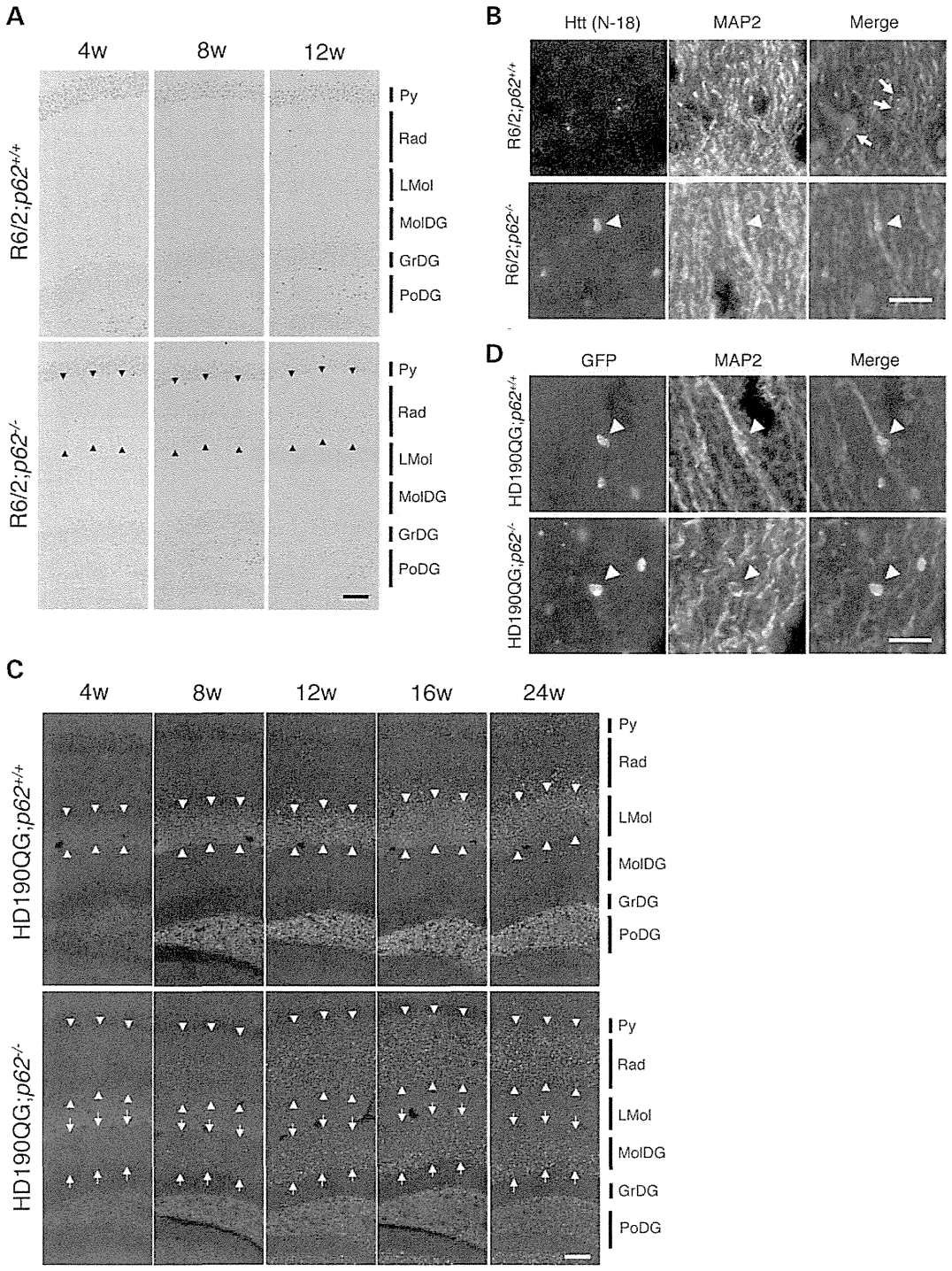

Figure 3. *p62* knockout increased extranuclear inclusions in two different HD model mice. (**A**) The hippocampus of R6/2 mice with and without *p62* was stained with anti-htt antibody (EM48). Extranuclear inclusions appear in the stratum radiatum of R6/2;$p62^{-/-}$ (arrowheads), but not in R6/2;$p62^{+/+}$. Hippocampal layers are indicated: Py, stratum pyramidale; Rad, stratum radiatum; LMol, lacunosum molecular layer; MolDG, molecular layer of the dentate gyrus; GrDG, granular layer dentate gyrus; PoDG, polymorgh layer of dentate gyrus. (**B**) Stratum radiatum of R6/2 mice with and without *p62* was stained with anti-htt (N-18) antibody (Alexa 488), anti-MAP2 antibody (Alexa 546) and DAPI. Nuclear inclusions (arrows) were observed in R6/2;$p62^{+/+}$. Extranuclear inclusions existed in dendrites of R6/2;$p62^{-/-}$ mice (arrowhead), but not in those of R6/2;$p62^{+/+}$. (**C**) The hippocampus of HD190QG mice with and without *p62* at 24 weeks of age was stained with anti-GFP antibody (Alexa 488) and DAPI. In HD190QG;$p62^{-/-}$, extranuclear inclusions appeared in the stratum radiatum (arrowheads) and the molecular layer of the dentate gyrus (arrows). On the other hand, in HD190QG;$p62^{+/+}$, extranuclear inclusions appeared in the LMol. (**D**) Stratum radiatum of HD190QG mice with and without *p62* was stained with anti-GFP antibody (Alexa 488), anti-MAP2 antibody (Alexa 546) and DAPI. Extranuclear inclusions existed in dendrites (arrowhead). Scale bar = 50 μm (A and C) and 10 μm (B and D).

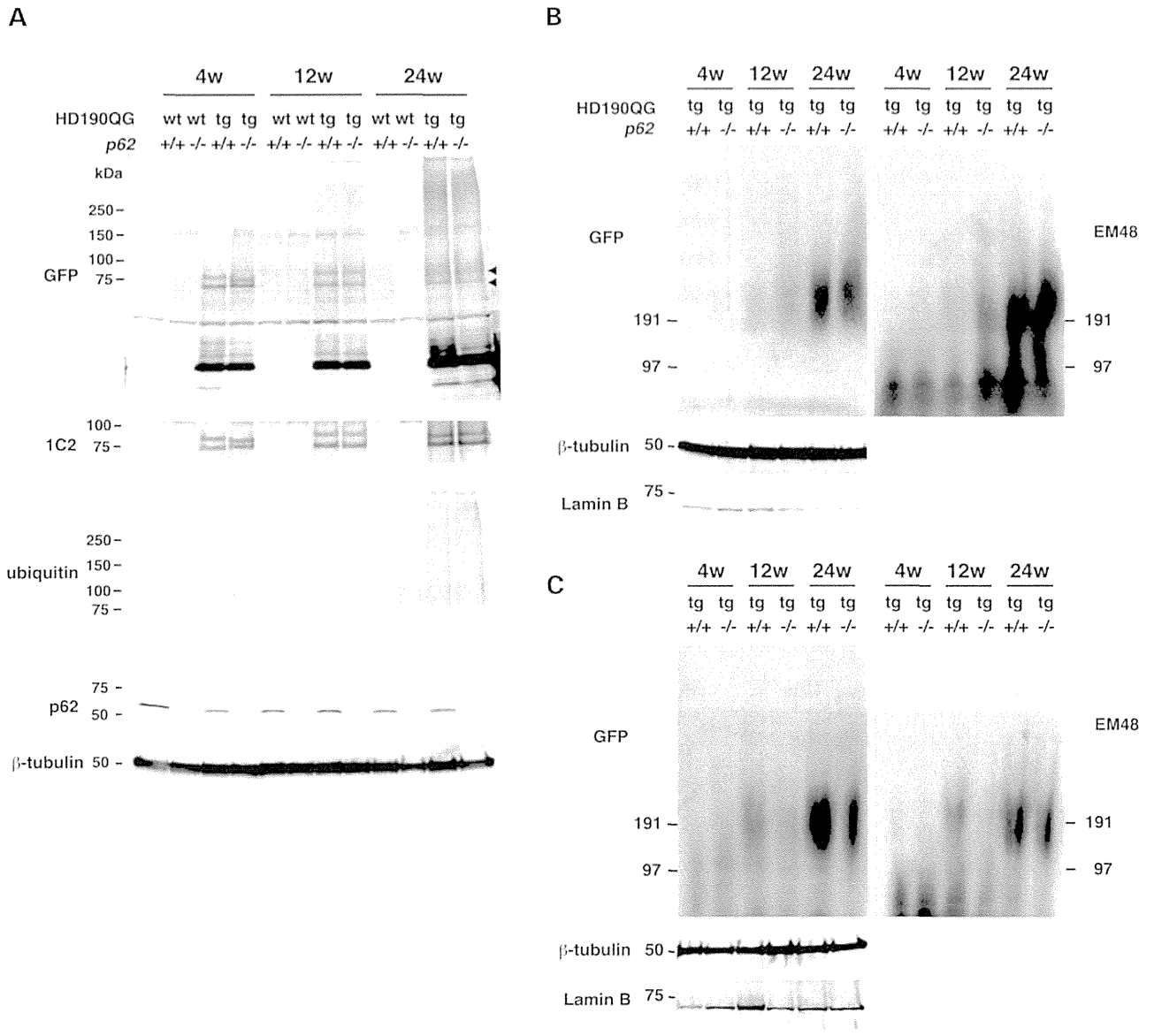

Figure 4. Immunoblot analysis of soluble and aggregated htt in total and nuclear fraction from HD190QG mice with and without *p62*. Brain samples were subjected to subcellular fractionation as described in Materials and Methods. (**A**) Total fractions were analyzed by western blot for soluble htt. There is no change in the amount of soluble htt (arrowheads) detected by anti-GFP or 1C2 antibody from HD190QG with and without *p62* at 4, 12 and 24 weeks of age. HD190QG mice have mutant htt transgenes with two different lengths of polyQ stretches. The sizes of these two bands were slightly different among HD190QG mice, because these mice show CAG-repeat length instability. The sizes of polyQ lengths of HD model mice used in this figure are described in Supplementary Material, Table S2. Knockout of *p62* was confirmed with anti-p62 antibody. (**B**) Total fractions were analyzed by AGERA. There was no difference between the htt protein complexes in the total fraction from HD190QG;$p62^{-/-}$ mice and that from HD190QG;$p62^{+/+}$. (**C**) Nuclear fractions were analyzed by AGERA. In nuclear fractions, the amount of aggregated htt from HD190QG;$p62^{-/-}$ mice was reduced at 12 and 24 weeks of age compared with that from HD190QG;$p62^{+/+}$. β-Tubulin was used as a marker for control protein (A–C) and Lamin B was used as a marker for nuclear membrane protein (B and C).

complex after 12 weeks of age (Fig. 4C), corresponding to the observed histological shift of inclusions from the nucleus to the cytoplasm.

p62 depletion extends the life span of HD model mice

We next examined whether *p62* knockout affects the life spans of R6/2, HD190QG and HD120QG mice. The life span of R6/2;$p62^{-/-}$ mice significantly increased with a mean survival time of 155 ± 4 days compared with 117 ± 3 days for R6/2; $p62^{-/+}$ mice and 123 ± 4 days for R6/2;$p62^{+/+}$ mice (Fig. 5A). The life span of HD190QG;$p62^{-/-}$ mice significantly increased with a mean survival time of 265 ± 11 days compared with 184 ± 7 days for both HD190QG;$p62^{-/+}$ and HD190QG;$p62^{+/+}$ mice (Fig. 5B). The life span of HD120QG;$p62^{-/-}$ mice significantly increased with a mean survival time of 415 ± 10 days

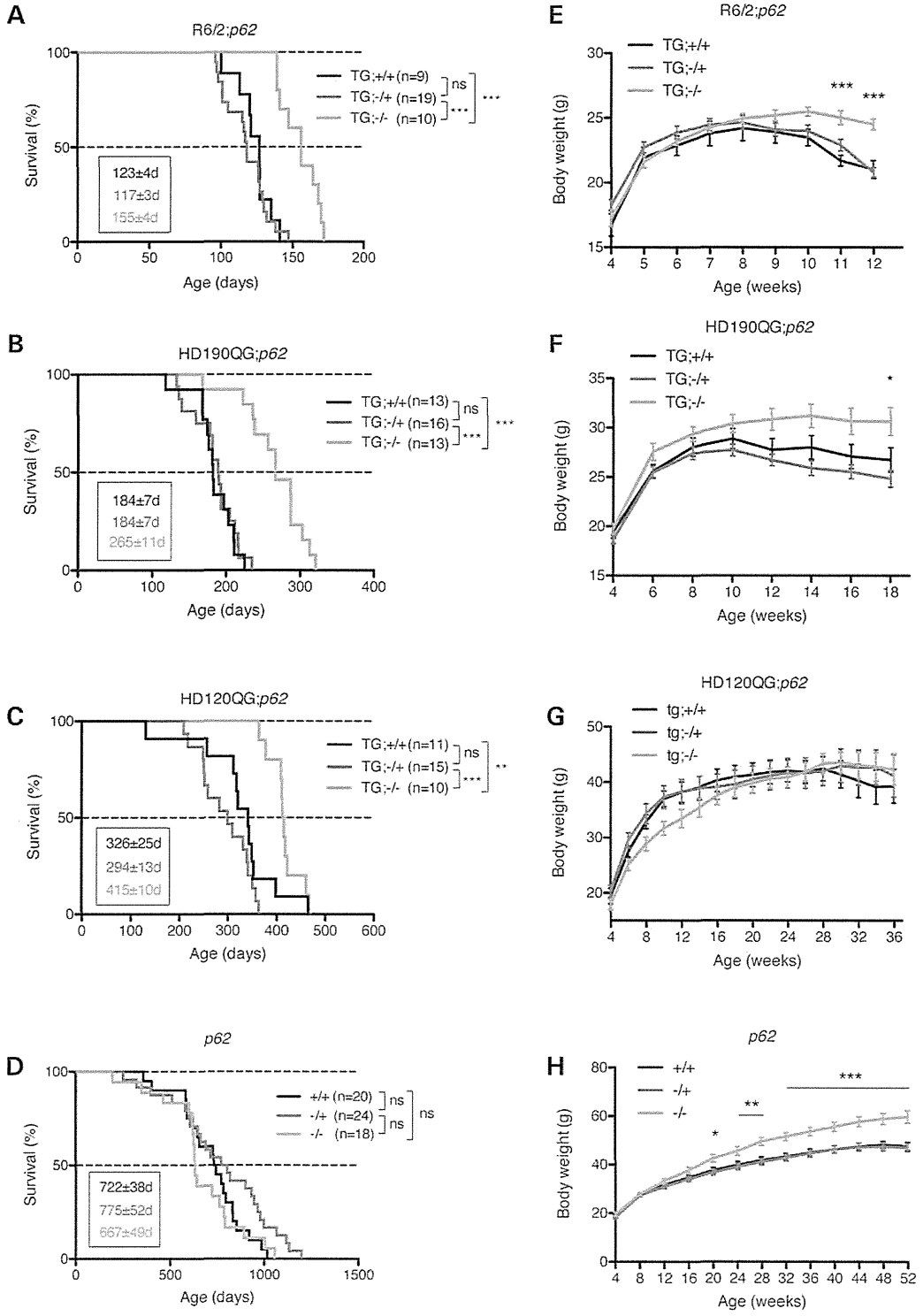

Figure 5. *p62* knockout increased life span in three different HD model mice and body weight in R6/2 and HD190QG mice, but not in HD120QG mice. (**A**) Mean survival time of R6/2;$p62^{-/-}$ was extended by 26% compared with that of R6/2;$p62^{+/+}$. (**B**) Mean survival time of HD190QG;$p62^{-/-}$ was extended by 44% compared with that of HD190QG;$p62^{+/+}$. (**C**) Mean survival time of HD120QG;$p62^{-/-}$ was extended by 27% compared with that of HD120QG;$p62^{+/+}$. (**D**) There was no difference in mean survival time among $p62^{+/+}$, $p62^{-/+}$ and $p62^{-/-}$ mice. These survival data were analyzed by the Kaplan–Meier method followed by a log-rank test with Bonferroni correction (significance level 0.05/3 = 0.0167). Mean ages ± SEM are provided. (**$P = 0.0098$, ***$P < 0.001$). (**E**) The body weight of R6/2;$p62^{-/-}$ mice was significantly greater than that of R6/2;$p62^{+/+}$ mice after 11 weeks of age. (**F**) The body weight of HD190QG;$p62^{-/-}$ mice was significantly greater than that of HD190QG;$p62^{+/+}$ mice after 18 weeks of age. (**G**) The body weight of HD120QG;$p62^{-/-}$ mice did not change significantly at each age compared with that of HD120QG;$p62^{+/+}$ mice. (**H**) The body weight of $p62^{-/-}$ mice was greater than that of $p62^{-/+}$ and $p62^{+/+}$ mice after 20 weeks of age. Means ± SEM are provided. (*$P<0.05$, **$P<0.01$, ***$P<0.001$), (E, F and H).

compared with 294 ± 13 days for HD120QG;$p62^{-/+}$ mice and 326 ± 25 days for HD120QG;$p62^{+/+}$ mice (Fig. 5C). There was no significant difference in life span among $p62^{+/+}$, $p62^{-/+}$ and $p62^{-/-}$ mice (Fig. 5D). *p62* knockout significantly extended the life spans of HD model mice, especially in HD190QG, which has longer polyQ proteins than HD120QG and R6/2. These data suggest that *p62* knockout may extend life span in a polyQ length-dependent manner, and that the extended life span is not due to the effect of *p62* knockout itself.

HD model mice normally show a progressive decrease in body weight. We next examined whether p62 knockout affects the body weight of R6/2, HD190QG and HD120QG mice. A delay in body weight loss was observed in *p62* knockout of R6/2 and HD190QG, but not in HD120QG, mice (Fig. 5E–G). The body weight of R6/2;$p62^{-/-}$ mice was significantly greater at 11 weeks of age compared with that of R6/2;$p62^{+/+}$ mice ($^{***}P < 0.001$) (Fig. 5E). The body weight of HD190QG;$p62^{-/-}$ mice was significantly greater at 18 weeks of age compared with that of HD190QG;$p62^{+/+}$ mice ($^{*}P < 0.05$) (Fig. 5F). $p62^{-/-}$ mice were reported to develop mature onset obesity (15,16). At 20 weeks, the average body weight of $p62^{-/-}$ mice without htt transgene became significantly greater than that of $p62^{+/+}$ and $p62^{-/+}$ mice (Fig. 5H).

Nuclear inclusions decrease and extranuclear inclusions increase in autophagy-deficient HD model mice

As stated above, we showed that nuclear inclusions in HD model mice decreased and life spans increased after depletion of p62, a protein that has an important role in selective autophagy. To examine whether these phenotypes result from deficiency of selective autophagy, we generated R6/2 mice with conditional knockout of *Atg5*, an essential gene for autophagosome formation. A transgenic mouse expressing Cre recombinase under the control of the synapsin I promoter (SynCre), which is expressed in neuronal cells as early as E12.5 (17), was used to generate $Atg5^{f/-}$;SynCre;R6/2 mice. Transgene expression in male SynCre mice occurs in germline recombination in progeny (18). The hippocampal CA3 region, in which Cre recombinase is expressed in almost all neuronal cells (19), was stained with EM48 (Fig. 6A), and the proportion of nuclei with inclusions was examined. There were significantly fewer nuclear inclusions in $Atg5^{f/-}$;SynCre;R6/2 compared with R6/2 mice (Fig. 6B). Next, we used magnified immunofluorescence images with EM48, the anti-ubiquitin antibody, and p62-C antibody to characterize these inclusions. In contrast to EM48-positive nuclear inclusions in R6/2 mice (Fig. 6D—n), nuclear inclusions decreased and extranuclear inclusions increased in the number of $Atg5^{f/-}$;SynCre;R6/2 (Fig. 6D—d and e). These extranuclear inclusions were subdivided into EM48-positive, ubiquitin-positive, and p62c-positive inclusions (Fig. 6D—e, arrows) and EM48-negative, ubiquitin-positive, and p62c-positive inclusions (Fig. 6D—e, arrowheads). The former inclusions could result from nucleation of mutant htt proteins followed by ubiquitination, and the latter inclusions could result from the accumulation of ubiquitinated proteins into the sequestosome that is a targeting unit for autophagosome entry. The change of inclusion formation in autophagy-deficient R6/2 mice was similar to that in *p62* knockout R6/2 mice. We previously reported that selective autophagy of the ubiquitinated proteins is enhanced by S403-phosphorylation of p62 (20). Therefore, we used immunohistochemistry in R6/2, $Atg5^{f/-}$;SynCre and $Atg5^{f/-}$;SynCre;R6/2 mice to determine whether p62 that colocalizes with ubiquitinated inclusions is S403-phosphorylated. Both types of extranuclear inclusions colocalized with S403-phos-p62 (Supplementary Material, Fig. S4A—c), but nuclear inclusions in R6/2 mice did not (Supplementary Material, Fig. S4A—i). We further examined the life spans of these mice. Despite fewer nuclear inclusions in $Atg5^{f/-}$;SynCre;R6/2 mice, the life span of $Atg5^{f/-}$;SynCre;R6/2 mice was significantly shorter, with a mean survival time of 86 ± 2 compared with 108 ± 4 days for $Atg5^{f/+}$;SynCre;R6/2 and 119 ± 10 days for $Atg5^{+/+}$;SynCre;R6/2 mice (Fig. 6C).

p62 knockout impairs protein degradation in cytoplasm but not in nucleus

To assess whether the depletion of *p62* affects protein degradation in the cytoplasm and nucleus, we prepared mouse embryonic fibroblast (MEF) $p62^{+/+}$, MEF $p62^{-/-}$ or MEF $p62^{-/-}$ expressing GFP-fused human wild-type p62 (G-p62) transfected with HD106Q-red fluorescent protein (RFP) or HD106Q-NLS-RFP. In cells transfected with HD106Q-RFP, inclusions mainly existed in the cytoplasm due to the nuclear export signal in the exon 1 of htt (21). The ratio of cells with inclusions to tranfected cells was greater in MEF $p62^{-/-}$ than in MEF $p62^{+/+}$; however, the proportion of cells with inclusions in MEF $p62^{-/-}$+G-p62 did not reach to that in MEF $p62^{+/+}$ (Fig. 7A and B). This was due to the fact that the expression level of endogenous p62 in MEF $p62^{+/+}$ is higher than that of transfected G-p62 (Supplementary Material, Fig. S6). On the other hand, in the cells transfected with HD106Q-NLS-RFP, inclusions appeared in the nucleus and there was no significant difference in the proportion of cells with nuclear inclusions among MEF $p62^{-/-}$, MEF $p62^{+/+}$ and MEF $p62^{-/-}$+G-p62. These data suggest that *p62* knockout impairs protein degradation in the cytoplasm but not in the nucleus.

DISCUSSION

In this study, we report that genetic ablation of *p62* in three kinds of HD model mice paradoxically ameliorates the disease phenotypes. The life span of HD model mice lacking *p62* was extended by 26, 44 and 27%, compared with those with *p62* (Fig. 5A–C). These extended life spans are not due to the effect of p62 knockout itself, because there was no significant difference in life span among $p62^{+/+}$, $p62^{-/+}$ and $p62^{-/-}$ mice. Regarding the body weight of these mice, significant delays in body weight loss were observed in *p62* knockout in R6/2 after 11 weeks of age and HD190QG mice after 18 weeks of age (Fig. 5E and F). On the other hand, the weight of $p62^{-/-}$ mice after 20 weeks of age was significantly greater than that of $p62^{+/+}$ mice (Fig. 5H). Therefore, the delays in body weight loss in R6/2;$p62^{-/-}$ and HD190QG;$p62^{-/-}$ mice were not due to the increased body weight after *p62* knockout; the significant increase in body weight in $p62^{-/-}$ mice was observed after those in R6/2;$p62^{-/-}$ and HD190QG;$p62^{-/-}$ mice. Immunohistochemical analysis revealed significantly fewer nuclear inclusions in HD model mice without p62, compared with HD model mice with p62 (Fig. 1). This was also confirmed biochemically in HD190QG using the

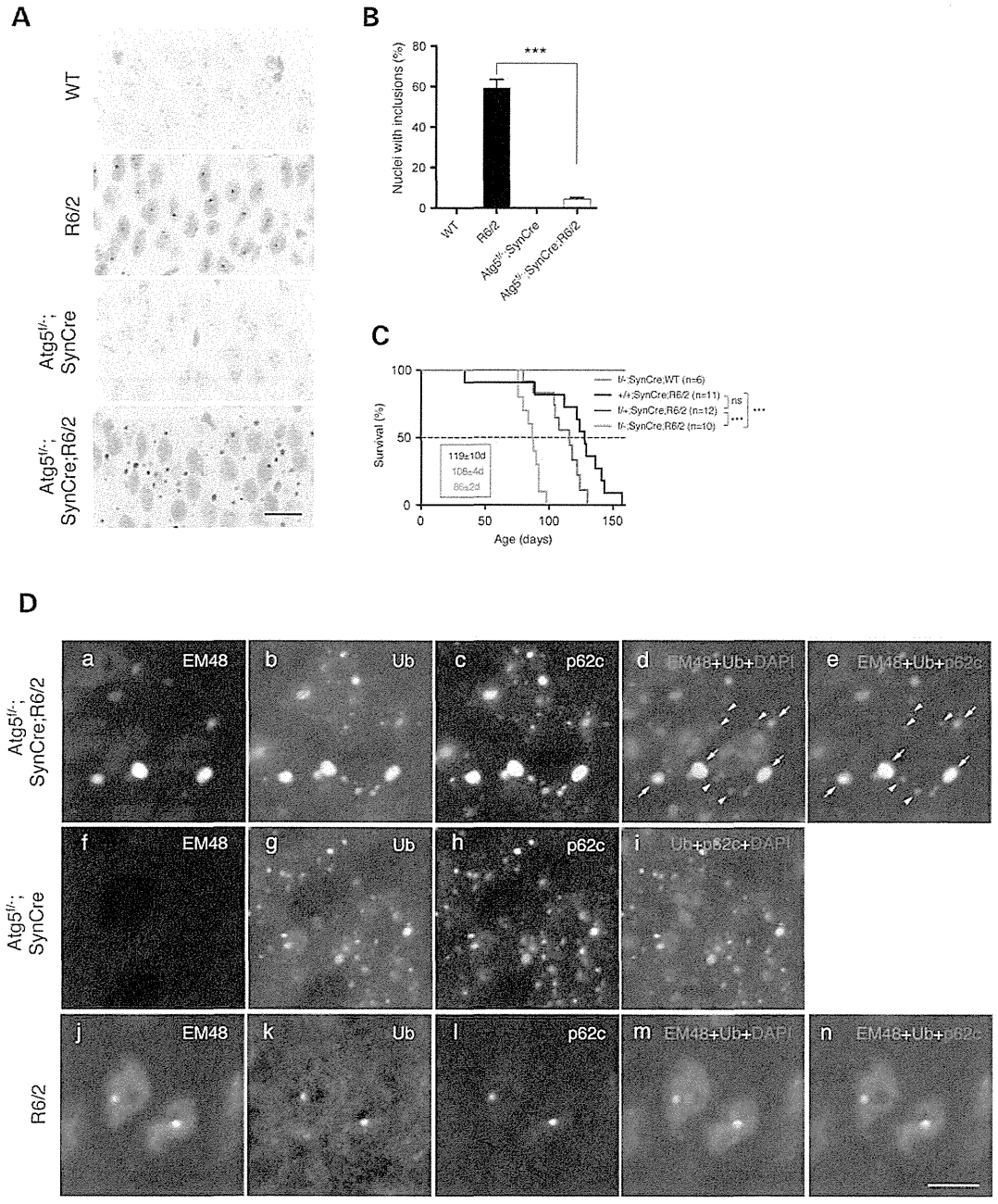

Figure 6. R6/2 mice with conditional knockout of *Atg5* by SynCre (*Atg5*$^{f/-}$;SynCre;R6/2) showed decreased nuclear inclusions and a shorter life span compared with R6/2. (**A**) The hippocampal CA3 of *Atg5*$^{f/-}$;SynCre;R6/2, *Atg5*$^{f/-}$;SynCre and R6/2 mice was stained with EM48 and counterstained with hematoxylin. (**B**) The percentage of the nuclei with inclusions, analyzing the immunostaining of the hippocampal CA3 with EM48. $n = 3$ for each genotype. (**C**) Mean survival time of *Atg5*$^{f/-}$;SynCre;R6/2 mice was decreased by 28% compared with that of R6/2 mice. These survival data were analyzed by a log-rank test with Bonferroni correction (significance level $0.05/3 = 0.0167$). Mean ages ± SEM are provided (***$P < 0.001$). (**D**) The hippocampal CA3 of *Atg5*$^{f/-}$;SynCre;R6/2 mice, *Atg5*$^{f/-}$;SynCre mice and R6/2 mice was stained with EM48 (EM48, Alexa488), anti-ubiquitin antibody (Ub, Alexa546), anti-p62-C antibody (p62c, Alexa647) and DAPI to confirm the localization of inclusions. Nuclear inclusions were detected in R6/2 mice (m), whereas these inclusions were hardly detected in *Atg5*$^{f/-}$;SynCre;R6/2 mice (d). Arrows and arrowheads in (d) show EM48-positive and ubiquitin-positive inclusions and EM48-negative and ubiquitin-positive inclusions, respectively. Extranuclear inclusions increased in *Atg5*$^{f/-}$;SynCre;R6/2 mice (d and e) compared with R6/2 mice (m and n). These inclusions can be subdivided into EM48-positive, ubiquitin-positive and p62c-positive inclusions (e, arrows) and EM48-negative, ubiquitin-positive and p62c-positive inclusions (e, arrowheads). Values are means ± SEM (***$P <$ 0.001). Scale bar = 20 μm (A) and 10 μm (D).

AGERA method (Fig. 4). It has been proposed that nuclear mutant htt may be toxic (22,23); therefore, the extended life span may be explained by a decrease in toxic nuclear mutant htt.

We also performed microarray analysis to examine whether transcriptional abnormalities in R6/2 changed by *p62* depletion. When comparing R6/2;*p62*$^{+/+}$ with R6/2;*p62*$^{-/-}$, we only

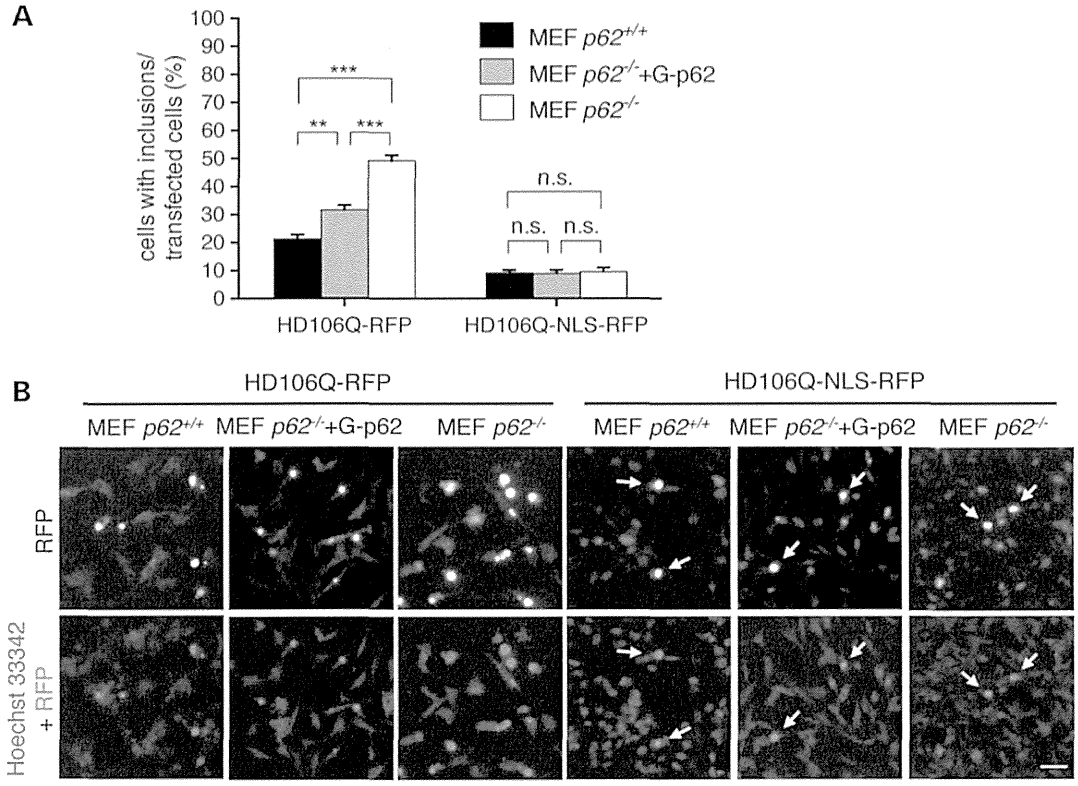

Figure 7. *p62* knockout impairs protein degradation in the cytoplasm, but not in the nucleus. (**A**) MEF $p62^{+/+}$, MEF $p62^{-/-}$ or MEF $p62^{-/-}$ +GFP-fused human wild-type p62 (G-p62) were transfected with HD106Q-RFP or HD106Q-NLS-RFP plasmids. The percentage of the cells with cytoplasmic inclusions after transfection of HD106Q-RFP increased in MEF $p62^{-/-}$ compared with MEF $p62^{+/+}$ and MEF $p62^{-/-}$ +G-p62 (***$P < 0.001$). When HD106Q-NLS-RFP was transfected, the cells with nuclear inclusions were not different among those cells. Values are means ± SEM (**$P < 0.01$, ***$P < 0.001$). (**B**) Fluorescence images of the above experiment. RFP fluorescence shows nuclear (arrows) and cytoplasmic inclusions in the cells transfected with HD106Q-RFP or HD106Q-NLS-RFP (upper panels). Nuclei were counterstained with Hoechst 33342 (lower panels). Values are means ± SEM. Scale bar = 50 μm.

found 12 genes with differential expression (five up-regulated and seven down-regulated; Supplementary Material, Fig. S5C and E). Moreover, we performed quantitative PCR of genes with previously known alteration in HD mice (Supplementary Material, Fig. S5A and B) (24–26), and we only found one gene, *Agxt2l1*, the expression level of which recovered by p62 depletion in R6/2;$p62^{-/-}$. Despite the decrease in nuclear inclusions, specific transcriptional changes were not observed in our experiment. In a previous study of environmental enrichment in R6/1 mice, no specific transcriptional changes were found, despite a decrease in nuclear inclusions (27). The effect of invisible aggregates on the transcriptional abnormality of early affected genes should be investigated further.

Autophagic degradation machinery works in the cytoplasm. Thus, we assumed that the decrease in nuclear inclusions correlated with an increase in cytoplasmic inclusions, which increased due to reduced protein clearance by loss of p62-dependent selective autophagy in the cytoplasm. To confirm this, we also examined R6/2 mice with *Atg5* depletion, which impairs autophagy in general. Similar to HD model mice without p62, nuclear inclusions almost disappeared in neurons in the region where Atg5 was deficient (Fig. 6A and B), but the life span of R6/2 mice with Atg5 depletion was shorter than that of R6/2 mice without *Atg5* depletion (Fig. 6C). Both *p62* and *Atg5* depletion induced decreases in nuclear inclusions. p62 controls selective autophagy and Atg5 controls more general autophagy including selective autophagy. Ubiquitinated substrates are degraded through selective autophagy, and p62 depletion results in accumulation of those selected substrates. However, Atg5 depletion might induce accumulation of more substrates in general, resulting in more toxic effects that could overcome the positive effect of decreased nuclear inclusions.

Cytoplasmic degradation of mutant htt was affected by p62 depletion, but its nuclear degradation was not (Fig. 7). Therefore, an increased accumulation of cytoplasmic mutant htt and a decrease in nuclear inclusions *in vivo* might be due to accelerated inclusion formation in the cytoplasm and a decrease of htt translocation into the nucleus after p62 depletion.

Similar findings to our study were observed in R6/2 mice with super-long CAG-repeat expansions (28). These mice also showed decreased nuclear inclusions, increased extranuclear inclusions and extended survival. It is thought that R6/2 mice have an upper threshold for forming nuclear inclusions, and when polyQ length is beyond the threshold, nuclear entry of mutant htt is blocked, resulting in decreased toxic nuclear inclusions and extended survival (28). This suggests that the decreased clearance of mutant htt due to the deficiency of p62 or Atg5 leads to increased cytoplasmic mutant htt and its

inclusions, even for the usual expanded polyQ length, resulting in decreased nuclear inclusions and extended survival as observed in R6/2 mice with super-long CAG-repeat expansions.

It has recently been reported that, in a transgenic mouse model of spinal and bulbar muscular atrophy (SBMA), another polyQ disease in which a mutant androgen receptor (AR) with an expanded polyQ repeat is toxic, *p62* depletion exacerbated motor phenotypes and the neuropathological outcome; overexpression of p62 protected the mice against mutant AR toxicity (29). *p62* depletion led to increased diffuse nuclear staining, whereas overexpressed p62 led to a decrease in diffuse staining and increased nuclear inclusions, suggesting a protective role of p62 and nuclear inclusions. These results were opposite to our results. This discrepancy may be due to the different tendencies for nuclear localization between mutant AR and mutant htt. AR easily translocates into the nucleus in the presence of androgen, but htt is basically a cytoplasmic protein. As shown in our study (Fig. 7), mutant htt with nuclear localization signal (NLS) showed no difference in nuclear inclusion formation with or without *p62*. For mutant htt without NLS, p62 depletion increased the cytoplasmic inclusions. In the case of mutant AR, it is stable with client proteins in the cytoplasm, but with androgen signal, mutant AR is freed from client proteins and moves into the nucleus as rapidly as mutant htt with NLS. Thus, there is no effect of p62 on cytoplasmic inclusion formation in SBMA model mice. Regarding the effect of p62 in the nucleus, we could not find the oligomers of mutant htt by immunohistochemistry as observed in SBMA mice and could not identify the shift from oligomers to nuclear inclusions. Using AGERA analysis in HD190QG without *p62* (Fig. 4C), we found fewer high-molecular-weight polyQ complexes in nuclear fraction, which may include oligomers. This could be explained, however, by the decrease of mutant htt in the nucleus due to cytoplasmic deposit. So, in conclusion, it is difficult to confirm that nuclear inclusion formation is protective. Rather it seems to be toxic, though we could not exclude the possible existence of an invisible oligomer in the nucleus.

In summary, we observed that *p62* depletion paradoxically ameliorates the phenotypes of HD model mice due to an increase in cytoplasmic inclusions and a decrease in nuclear inclusions. This result suggests that mutant htt is degraded through autophagy in the cytoplasm, and loss of this quality control system increases cytoplasmic inclusions and decreases nuclear inclusions. The regulation for this system has been considered a possible therapeutic target, although this paradoxical effect requires further investigation.

MATERIALS AND METHODS

Mice

Three HD model mice (R6/2, HD190QG and HD120QG), *p62* knockout mice and *Atg5* conditional knockout mice were used in this study. Heterozygous *HTT* exon 1 transgenic mice of the R6/2 strain (121–133 CAG-repeats) were used for our *in vivo* study (30). The HD190QG mice harbor two mutant truncated N-terminal htt containing around 120 and 190 CAG repeats fused with EGFP in its genome (31). HD120QG mice were generated by selecting mice with shorter CAG repeats from the HD190QG line. HD120QG mice show a milder phenotype compared with HD190QG mice. The polyQ lengths were slightly different among HD190QG and HD120QG mice, because these mice show CAG repeat length instability. Precise sizes of polyQ lengths of HD model mice used in each experiment are described in Supplementary Material, Table S2. *p62* knockout mice used in this study were described previously (11). *Atg5* conditional knockout mice were kindly provided by Professor Noboru Mizushima (9). R6/2 and Synapsin I-Cre (SynCre) transgenic mice [B6.Cg-Tg(Syn1-cre)671Jxm/J] were obtained from the Jackson Laboratory (Bar Harbor, ME, USA) (17). All mouse experiments were approved by the Animal Experiment Committee of the RIKEN Brain Science Institute.

Generation of htt transgenic/*p62* knockout mice and genotyping

The ovaries of R6/2 mice were transplanted into B6CBAF1 female mice and the ovaries of HD190QG or HD120QG mice were transplanted into BDF1 female mice. Those female mice were mated with homozygous *p62* knockout male mice of the B6 strain. The female offspring (R6/2;$p62^{-/+}$, HD190 QG;$p62^{-/+}$ or HD120QG;$p62^{-/+}$) were mated with heterozygous *p62* knockout male mice to produce all the genotype combinations. Genotyping PCR and determination of CAG-repeat number of HD model mice were performed as described previously (31). Genotyping PCR of *p62* knockout mice was performed with two primer pairs: 5′-CTGCATGTCTTCTCCCATGAC-3′/5′-TAGATACCTAGGTGAGCTCTG-3′ and 5′-CTTACGGGT CCTTTTCCCAAC-3′/5′-TCCTCCTTGCCCAGAAGATAG-3′.

Generation of htt transgenic/*Atg5* conditional knockout mice and genotyping

The ovaries of R6/2 were transplanted into B6CBAF1 female mice. Those female mice were mated with $Atg5^{f/f}$ male mice. Female offspring (R6/2;$Atg5^{f/+}$) were mated with $Atg5^{f/+}$;SynCre to produce all the genotype combinations. Genotyping PCR of $Atg5^{flox}$ alleles and the Cre-recombinase transgene was performed as described previously (9).

Antibodies

The following antibodies were used: mouse anti-htt; EM48 (MAB5374, Chemicon, Temecula, CA, USA), anti-htt; N-18 (sc-8767, Santa Cruz Biotechnologies, Dallas, TX, USA), mouse anti-polyQ; 1C2 (MAB1574, Chemicon), guinea pig anti-p62 (p62-C, GP62-C, Progen, Heidelberg, Germany), rabbit anti-p62 (PM045, MBL, Nagoya, Japan), rat anti-S403-phosphorylated p62 (S403-phos-p62, D343-3, MBL), chicken anti-GFP (ab13970, Abcam, Cambridge, UK), rabbit anti-GFP (A6455, Molecular Probe, Eugene, OR, USA), rabbit anti-ubiquitin (Z0452, DAKO, Copenhagen, Denmark), mouse anti-MAP2 (M9942, Sigma-Aldrich, Saint Louis, MO, USA), goat anti-Lamin B (M-20, Santa Cruz Biotechnologies), anti-β-tubulin (T4026, Sigma-Aldrich) and Alexa-conjugated secondary antibodies (Invitrogen, Carlsbad, CA, USA).

Immunohistochemistry and immunofluorescence staining

Mice were anesthetized and immediately fixed by perfusion through the left ventricle with 4% paraformaldehyde in PBS.

A brain was collected, postfixed with the same fixative overnight and processed for embedding. Paraffin-embedded brain sections (5 μm thickness) were deparaffinized, autoclaved in 10 mM citrate buffer (pH 6.0) at 120°C for 5 min and immunostainings were performed as described in our previous study (32–34). The primary antibodies were diluted as follows: 1 : 500 for anti-htt (EM48), anti-GFP, anti-ubiquitin and anti-S403-phos-p62, 1 : 1000 for anti-p62-C and 1 : 300 for anti-MAP2 and anti-htt (N-18). Alexa-conjugated secondary antibodies were diluted at 1 : 300.

Imaging and counting inclusions

Images were obtained with a BZ9000 digital microscopic system (KEYENCE, Osaka, Japan) and a TCS SP5 confocal system (Leica, Heidelberg, Germany). Inclusions were stained with anti-htt antibody (EM48) and anti-GFP antibody. Nuclei were stained with DAPI. The percentages of nuclei with inclusions were calculated and averaged from three mice of each genotype.

Preparation of total and nuclear fraction

Homogenization and fractionation of mice cerebrum were performed as described previously (31). Mouse brains were homogenized in nine volumes (v/w) of 0.25 M sucrose/buffer A (50 mM Tris–HCl, pH 7.4, 5 mM $MgCl_2$, 2 mM dithiothreitol and 1 mM phenylmethylsulfonyl), supplemented with complete EDTA-free protease inhibitor cocktail tablets (Roche Diagnostics, Mannheim, Germany) in a digital homogenizer (As One, Osaka, Japan) using eight strokes at 1000 rpm. A portion of the homogenate was briefly sonicated and used as the total lysate, and the rest of the homogenate was centrifuged at 1000 *g* for 10 min at 4°C. The pellets were resuspended and homogenized in 5 ml of 2.1 M sucrose/buffer A by five strokes at 1000 rpm with a digital homogenizer. Nuclei were sedimented by centrifugation at 8000 *g* for 80 min at 4°C. The pellet containing the nuclei was resuspended in 0.5 ml of 10 mM Tris–HCl (pH 7.4) and 2 mM $MgCl_2$ with the protease inhibitors.

Immunoblotting

The lysates or fractions were boiled in SDS sample buffer and subjected to western blot analysis as described previously (34).

Agarose gel electrophoresis for resolving aggregates

Agarose was dissolved in gel buffer (100 mM Tris and 100 mM glycine) by boiling, and then the 1% agarose solution was cooled to a moderate temperature and poured into the gel plates of PAGEL (ATTO, Tokyo, Japan), of which the sides and the bottom had been tightly sealed with a plastic tape. Immediately, a plastic comb was inserted at the top. After cooling to room temperature, the gel was used immediately or stored at 4°C. Before setting the gel into the apparatus for electrophoresis, the plastic tape was removed. Electrophoresis was performed using an apparatus for PAGEL (AE-6530P, ATTO) at 50 V for 1 h at room temperature with running buffer (100 mM Tris, 100 mM glycine and 0.1% SDS). When necessary, HiMark prestained protein standard (Life Technologies, Carlsbad, CA, USA) was loaded as a size marker. For western analysis, proteins were transferred onto a polyvinylidene fluoride membrane for 90 min at 40 V, 4°C or 150 mA at room temperature. Immunodetection was performed as in conventional western analysis.

DNA transfection into MEF $p62^{-/-}$ cells and counting inclusions

MEF $p62^{-/-}$ and $p62^{+/+}$ cells were generated from $p62^{-/-}$ and $p62^{+/+}$ mice, and immortalized with SV40T antigen (kind gift from Dr Yusuke Yanagi, Kyushu University). G-p62 (20) was cloned into a pJTI vector (Jump-in system; Invitrogen). pJTI-G-p62 was then stably transfected into the subcloned immortalized MEF $p62^{-/-}$ cells. G-p62 expression in the single colony of MEF $p62^{-/-}$ +G-p62 cells was confirmed by western blotting using p62 antibody. The htt exon 1 with 106 CAG repeats (HD106Q) was cloned into the N-terminal of monomeric RFP (HD106Q-RFP), and three repeats of NLS sequence (GGATCCACCAAAAAAGAAGAGAAAGGTAG ATCT) were introduced at a *Bam*HI site between HD106Q and RFP (HD106Q-NLS-RFP). CAG-repeat numbers and entire htt exon 1 sequences were confirmed. HD106Q-RFP or HD106Q-NLS-RFP plasmids were transfected into MEF $p62^{-/-}$, MEF $p62^{-/-}$ +G-p62 or MEF $p62^{+/+}$ cells with lipofectamine 2000 (Invitrogen). Cells were fixed with formaldehyde 3 days after transfection and RFP were visualized by fluorescent microscopy using Keyence BZ-9000 equipped with a 20× dry objective lens. RFP-transfected cells and inclusions in five different microscopic fields were separately counted using the Keyence software.

Statistical analysis

We used unpaired Student's *t*-test for comparison between two sample groups. One-way ANOVA followed by the Tukey test was used for multiple comparisons. For survival rate, we plotted the survival distribution curve with the Kaplan–Meier method followed by a log-rank test and with Bonferroni correction. We generated these data with Prism5 (GraphPad Software, La Jolla, CA, USA). We considered the difference between comparisons to be significant when $P < 0.05$ for all the statistical analyses except for the survival analysis.

AUTHORS' CONTRIBUTIONS

M.K., G.M. and Y.K. performed the main experiments. M.O., M.K.-Y., C.W. and H.T. conducted some supportive experiments. T.Y. and E.W. provided p62 knockout mice and K.N. performed the initial experiments. M.K., T.Sh., T.Sa., N.H. and N.N. analyzed data. M.K. and N.N. designed experiments and wrote the manuscript. N.N. organized the whole project.

SUPPLEMENTARY MATERIAL

Supplementary Material is available at *HMG* online.

ACKNOWLEDGEMENTS

We thank Professor Noboru Mizushima (University of Tokyo) for *Atg5* knockout mice, Dr Yusuke Yanagi (Kyushu University)

for SV40T antigen. We thank Mses Tomoko Yoda and Itsuko Yamamoto and the staff at the RRC (RIKEN BSI), and Laboratory of Morphology and Image Analysis and Laboratory of Molecular and Biochemical Research, Research Support Center (Juntendo University Graduate School of Medicine).

Conflict of Interest statement. None declared.

FUNDING

This work was supported by a grant-in-aid from the Ministry of Education, Culture, Sports, Science and Technology (MEXT) of Japan to N.N. (22110004, 22240037, 24659436 and 25253066), by CREST from JST to N.N. and by a grant-in-aid for the Research on Measures for Ataxic Diseases from the Ministry of Health, Welfare and Labor to N.N.

REFERENCES

1. Yamamoto, A. and Simonsen, A. (2011) The elimination of accumulated and aggregated proteins: a role for aggrephagy in neurodegeneration. *Neurobiol. Dis.*, **43**, 17–28.
2. Bauer, P.O. and Nukina, N. (2009) The pathogenic mechanisms of polyglutamine diseases and current therapeutic strategies. *J. Neurochem.*, **110**, 1737–1765.
3. Kraft, C., Peter, M. and Hofmann, K. (2010) Selective autophagy: ubiquitin-mediated recognition and beyond. *Nat. Cell Biol.*, **12**, 836–841.
4. Nagaoka, U., Kim, K., Jana, N.R., Doi, H., Maruyama, M., Mitsui, K., Oyama, F. and Nukina, N. (2004) Increased expression of p62 in expanded polyglutamine-expressing cells and its association with polyglutamine inclusions. *J. Neurochem.*, **91**, 57–68.
5. Kuusisto, E., Salminen, A. and Alafuzoff, I. (2001) Ubiquitin-binding protein p62 is present in neuronal and glial inclusions in human tauopathies and synucleinopathies. *Neuroreport*, **12**, 2085–2090.
6. Mizuno, Y., Amari, M., Takatama, M., Aizawa, H., Mihara, B. and Okamoto, K. (2006) Immunoreactivities of p62, an ubiqutin-binding protein, in the spinal anterior horn cells of patients with amyotrophic lateral sclerosis. *J. Neurol. Sci.*, **249**, 13–18.
7. Nakaso, K., Yoshimoto, Y., Nakano, T., Takeshima, T., Fukuhara, Y., Yasui, K., Araga, S., Yanagawa, T., Ishii, T. and Nakashima, K. (2004) Transcriptional activation of p62/A170/ZIP during the formation of the aggregates: possible mechanisms and the role in Lewy body formation in Parkinson's disease. *Brain Res.*, **1012**, 42–51.
8. Rue, L., Lopez-Soop, G., Gelpi, E., Martinez-Vicente, M., Alberch, J. and Perez-Navarro, E. (2013) Brain region- and age-dependent dysregulation of p62 and NBR1 in a mouse model of Huntington's disease. *Neurobiol. Dis.*, **52**, 219–228.
9. Hara, T., Nakamura, K., Matsui, M., Yamamoto, A., Nakahara, Y., Suzuki-Migishima, R., Yokoyama, M., Mishima, K., Saito, I., Okano, H. *et al.* (2006) Suppression of basal autophagy in neural cells causes neurodegenerative disease in mice. *Nature*, **441**, 885–889.
10. Komatsu, M., Waguri, S., Chiba, T., Murata, S., Iwata, J., Tanida, I., Ueno, T., Koike, M., Uchiyama, Y., Kominami, E. *et al.* (2006) Loss of autophagy in the central nervous system causes neurodegeneration in mice. *Nature*, **441**, 880–884.
11. Komatsu, M., Waguri, S., Koike, M., Sou, Y.S., Ueno, T., Hara, T., Mizushima, N., Iwata, J., Ezaki, J., Murata, S. *et al.* (2007) Homeostatic levels of p62 control cytoplasmic inclusion body formation in autophagy-deficient mice. *Cell*, **131**, 1149–1163.
12. Korolchuk, V.I., Mansilla, A., Menzies, F.M. and Rubinsztein, D.C. (2009) Autophagy inhibition compromises degradation of ubiquitin-proteasome pathway substrates. *Mol. Cell*, **33**, 517–527.
13. Babu, J.R., Geetha, T. and Wooten, M.W. (2005) Sequestosome 1/p62 shuttles polyubiquitinated tau for proteasomal degradation. *J. Neurochem.*, **94**, 192–203.
14. Weiss, A., Klein, C., Woodman, B., Sathasivam, K., Bibel, M., Regulier, E., Bates, G.P. and Paganetti, P. (2008) Sensitive biochemical aggregate detection reveals aggregation onset before symptom development in cellular and murine models of Huntington's disease. *J. Neurochem.*, **104**, 846–858.
15. Okada, K., Yanagawa, T., Warabi, E., Yamastu, K., Uwayama, J., Takeda, K., Utsunomiya, H., Yoshida, H., Shoda, J. and Ishii, T. (2009) The alpha-glucosidase inhibitor acarbose prevents obesity and simple steatosis in sequestosome 1/A170/p62 deficient mice. *Hepatol. Res.*, **39**, 490–500.
16. Harada, H., Warabi, E., Matsuki, T., Yanagawa, T., Okada, K., Uwayama, J., Ikeda, A., Nakaso, K., Kirii, K., Noguchi, N. *et al.* (2013) Deficiency of p62/sequestosome 1 causes hyperphagia due to leptin resistance in the brain. *J. Neurosci.*, **33**, 14767–14777.
17. Zhu, Y., Romero, M.I., Ghosh, P., Ye, Z., Charnay, P., Rushing, E.J., Marth, J.D. and Parada, L.F. (2001) Ablation of NF1 function in neurons induces abnormal development of cerebral cortex and reactive gliosis in the brain. *Genes Dev.*, **15**, 859–876.
18. Rempe, D., Vangeison, G., Hamilton, J., Li, Y., Jepson, M. and Federoff, H.J. (2006) Synapsin I Cre transgene expression in male mice produces germline recombination in progeny. *Genesis*, **44**, 44–49.
19. Yamanaka, T., Tosaki, A., Kurosawa, M., Akimoto, K., Hirose, T., Ohno, S., Hattori, N. and Nukina, N. (2013) Loss of aPKClambda in differentiated neurons disrupts the polarity complex but does not induce obvious neuronal loss or disorientation in mouse brains. *PloS ONE*, **8**, e84036.
20. Matsumoto, G., Wada, K., Okuno, M., Kurosawa, M. and Nukina, N. (2011) Serine 403 phosphorylation of p62/SQSTM1 regulates selective autophagic clearance of ubiquitinated proteins. *Mol. Cell*, **44**, 279–289.
21. Maiuri, T., Woloshansky, T., Xia, J. and Truant, R. (2013) The huntingtin N17 domain is a multifunctional CRM1 and Ran-dependent nuclear and cilial export signal. *Hum. Mol. Genet.*, **22**, 1383–1394.
22. Peters, M.F., Nucifora, F.C. Jr, Kushi, J., Seaman, H.C., Cooper, J.K., Herring, W.J., Dawson, V.L., Dawson, T.M. and Ross, C.A. (1999) Nuclear targeting of mutant Huntingtin increases toxicity. *Mol. Cell. Neurosci.*, **14**, 121–128.
23. Saudou, F., Finkbeiner, S., Devys, D. and Greenberg, M.E. (1998) Huntingtin acts in the nucleus to induce apoptosis but death does not correlate with the formation of intranuclear inclusions. *Cell*, **95**, 55–66.
24. Ferrante, R.J., Kubilus, J.K., Lee, J., Ryu, H., Beesen, A., Zucker, B., Smith, K., Kowall, N.W., Ratan, R.R., Luthi-Carter, R. *et al.* (2003) Histone deacetylase inhibition by sodium butyrate chemotherapy ameliorates the neurodegenerative phenotype in Huntington's disease mice. *J. Neurosci.*, **23**, 9418–9427.
25. Gardian, G., Browne, S.E., Choi, D.K., Klivenyi, P., Gregorio, J., Kubilus, J.K., Ryu, H., Langley, B., Ratan, R.R., Ferrante, R.J. *et al.* (2005) Neuroprotective effects of phenylbutyrate in the N171–82Q transgenic mouse model of Huntington's disease. *J. Biol. Chem.*, **280**, 556–563.
26. Seredenina, T. and Luthi-Carter, R. (2012) What have we learned from gene expression profiles in Huntington's disease? *Neurobiol. Dis.*, **45**, 83–98.
27. Benn, C.L., Luthi-Carter, R., Kuhn, A., Sadri-Vakili, G., Blankson, K.L., Dalai, S.C., Goldstein, D.R., Spires, T.L., Pritchard, J., Olson, J.M. *et al.* (2010) Environmental enrichment reduces neuronal intranuclear inclusion load but has no effect on messenger RNA expression in a mouse model of Huntington disease. *J. Neuropathol. Exp. Neurol.*, **69**, 817–827.
28. Morton, A.J., Glynn, D., Leavens, W., Zheng, Z., Faull, R.L., Skepper, J.N. and Wight, J.M. (2009) Paradoxical delay in the onset of disease caused by super-long CAG repeat expansions in R6/2 mice. *Neurobiol. Dis.*, **33**, 331–341.
29. Doi, H., Adachi, H., Katsuno, M., Minamiyama, M., Matsumoto, S., Kondo, N., Miyazaki, Y., Iida, M., Tohnai, G., Qiang, Q. *et al.* (2013) p62/SQSTM1 differentially removes the toxic mutant androgen receptor via autophagy and inclusion formation in a spinal and bulbar muscular atrophy mouse model. *J. Neurosci.*, **33**, 7710–7727.
30. Mangiarini, L., Sathasivam, K., Seller, M., Cozens, B., Harper, A., Hetherington, C., Lawton, M., Trottier, Y., Lehrach, H., Davies, S.W. *et al.* (1996) Exon 1 of the HD gene with an expanded CAG repeat is sufficient to cause a progressive neurological phenotype in transgenic mice. *Cell*, **87**, 493–506.
31. Kotliarova, S., Jana, N.R., Sakamoto, N., Kurosawa, M., Miyazaki, H., Nekooki, M., Doi, H., Machida, Y., Wong, H.K., Suzuki, T. *et al.* (2005) Decreased expression of hypothalamic neuropeptides in Huntington disease transgenic mice with expanded polyglutamine-EGFP fluorescent aggregates. *J. Neurochem.*, **93**, 641–653.

32. Wong, H.K., Bauer, P.O., Kurosawa, M., Goswami, A., Washizu, C., Machida, Y., Tosaki, A., Yamada, M., Knopfel, T., Nakamura, T. *et al.* (2008) Blocking acid-sensing ion channel 1 alleviates Huntington's disease pathology via an ubiquitin-proteasome system-dependent mechanism. *Hum. Mol. Genet.*, **17**, 3223–3235.
33. Yamanaka, T., Tosaki, A., Miyazaki, H., Kurosawa, M., Furukawa, Y., Yamada, M. and Nukina, N. (2010) Mutant huntingtin fragment selectively suppresses Brn-2 POU domain transcription factor to mediate hypothalamic cell dysfunction. *Hum. Mol. Genet.*, **19**, 2099–2112.
34. Bauer, P.O., Goswami, A., Wong, H.K., Okuno, M., Kurosawa, M., Yamada, M., Miyazaki, H., Matsumoto, G., Kino, Y., Nagai, Y. *et al.* (2010) Harnessing chaperone-mediated autophagy for the selective degradation of mutant huntingtin protein. *Nat. Biotechnol.*, **28**, 256–263.

PLOS ONE

Large-Scale RNA Interference Screening in Mammalian Cells Identifies Novel Regulators of Mutant Huntingtin Aggregation

Tomoyuki Yamanaka[1,2,3,6☯], Hon Kit Wong[2,4☯], Asako Tosaki[2], Peter O. Bauer[2], Koji Wada[2], Masaru Kurosawa[1,2,3,6], Tomomi Shimogori[3], Nobutaka Hattori[5], Nobuyuki Nukina[1,2,3,6*]

1 Department of Neuroscience for Neurodegenerative Disorders, Juntendo University Graduate School of Medicine, Tokyo, Japan, **2** Laboratory for Structural Neuropathology, RIKEN Brain Science Institute, Saitama, Japan, **3** Laboratory for Molecular Mechanisms of Thalamus Development, RIKEN Brain Science Institute, Saitama, Japan, **4** Center for Neurologic Diseases, Department of Neurology, Brigham and Women's Hospital and Harvard Medical School, Harvard Institutes of Medicine, Boston, Massachusetts, United States of America, **5** Department of Neurology, Juntendo University Graduate School of Medicine, Tokyo, Japan, **6** CREST (Core Research for Evolutionary Science and Technology), JST, Tokyo, Japan

Abstract

In polyglutamine (polyQ) diseases including Huntington's disease (HD), mutant proteins containing expanded polyQ stretch form aggregates in neurons. Genetic or RNAi screenings in yeast, *C. elegans* or *Drosophila* have identified multiple genes modifying polyQ aggregation, a few of which are confirmed effective in mammals. However, the overall molecular mechanism underlying polyQ protein aggregation in mammalian cells still remains obscure. We here perform RNAi screening in mouse neuro2a cells to identify mammalian modifiers for aggregation of mutant huntingtin, a causative protein of HD. By systematic cell transfection and automated cell image analysis, we screen ~12000 shRNA clones and identify 111 shRNAs that either suppress or enhance mutant huntingtin aggregation, without altering its gene expression. Classification of the shRNA-targets suggests that genes with various cellular functions such as gene transcription and protein phosphorylation are involved in modifying the aggregation. Subsequent analysis suggests that, in addition to the aggregation-modifiers sensitive to proteasome inhibition, some of them, such as a transcription factor Tcf20, and kinases Csnk1d and Pik3c2a, are insensitive to it. As for Tcf20, which contains polyQ stretches at N-terminus, its binding to mutant huntingtin aggregates is observed in neuro2a cells and in HD model mouse neurons. Notably, except Pik3c2a, the rest of the modifiers identified here are novel. Thus, our first large-scale RNAi screening in mammalian system identifies previously undescribed genetic players that regulate mutant huntingtin aggregation by several, possibly mammalian-specific mechanisms.

Citation: Yamanaka T, Wong HK, Tosaki A, Bauer PO, Wada K, et al. (2014) Large-Scale RNA Interference Screening in Mammalian Cells Identifies Novel Regulators of Mutant Huntingtin Aggregation. PLoS ONE 9(4): e93891. doi:10.1371/journal.pone.0093891

Editor: Yoshitaka Nagai, National Center of Neurology and Psychiatry, Japan

Received August 19, 2013; **Accepted** March 10, 2014; **Published** April 4, 2014

Funding: This work was supported by a Grant-in-Aid from Ministry of Education, Culture, Sports, Science and Technology (MEXT) of Japan for TY (24111553, 23700430) and NN (22110004, 22240037, 24659436); by Life Science Foundation of Japan for TY; by Mochida Memorial Foundation for Medical and Pharmaceutical Research for TY; by CREST from JST for NN; and by Grant-in-Aid for the Research on Measures for Ataxic Diseases from the Ministry of Health, Welfare and Labor for NN. The funders had no role in study design, data collection and analysis, decision to publish, or preparation of the manuscript.

Competing Interests: The authors have declared that no competing interests exist.

* E-mail: nnukina@juntendo.ac.jp

☯ These authors contributed equally to this work.

Introduction

Polyglutamine (polyQ) diseases are adult-onset hereditary neurodegenerative disorders. These include Huntington's disease (HD), spinocerebellar ataxias (SCA1, 2, 3, 6, 7, 17), dentatorubral-pallidoluysian atrophy (DRPLA) and spinobulbar muscular atrophy (SBMA). The polyQ diseases are caused by expansion of CAG repeats in certain causative genes. The mutant proteins containing expanded polyQ stretch are misfolded and aggregated, leading to formation of nuclear inclusions in neurons [1,2].

The polyQ protein aggregation accompanies sequestration of several cellular components such as transcription factors [3–7] and RNA binding proteins [8,9], leading to dysregulation of gene expression during neurodegeneration [10–12]. In addition, polyQ-mediated cell toxicity is reported to be reduced through suppressing polyQ aggregation by chaperones [13–18], chaperonin [19–21], QBP1 (polyQ-binding peptide 1) [22,23], or chemical compounds such as Congo Red [24] or trehalose [25]. Thus, examination of molecular mechanisms underlying polyQ aggregation is one of the effective strategies for understanding pathomechanism of and searching therapeutic targets for polyQ diseases.

In past 10 years, several groups have performed genetic or RNA interference (RNAi) screening to identify polyQ aggregation-modifying genes using yeast [26], *C. elegans* [27–30] or *Drosophila* models [31–34]. These screenings have identified genes in various contexts such as transcription, RNA processing, protein transport and signal transduction, in addition to protein folding and degradation. These observations suggest that multiple cellular pathways are involved in the regulation of polyQ protein aggregation in non-mammalian systems. Although a few of their orthologues are shown to modify polyQ protein aggregation in

mammalian cells [26,34], a large-scale, systematic screen has not been performed in any mammalian systems and the overall molecular mechanism underlying polyQ protein aggregation in mammalian cells remains obscure.

To this end, we perform RNAi screening in mouse neuroblastoma cells to attempt to identify novel aggregation-modifiers for mutant huntingtin (Htt), a causative protein of HD, in mammals. To the best of our knowledge, this is the first comprehensive analysis of polyQ aggregation-modifying genes in mammals. We transduce ~12000 short hairpin RNA (shRNA) clones into neuro2a cells that inducibly express mutant Htt, and analyze the aggregation by automated quantitative fluorescence microscopy. After three screenings, we identify 111 shRNAs that specifically modify the mutant Htt aggregation in neuro2a cells. Subsequent analyses suggest that the modifications can be mediated by several mechanisms, that is, by direct/indirect regulation through proteasome-dependent/-independent pathways. Importantly, all of the shRNA targets except of one gene [33] are not found by previous screenings using other organisms described above. Thus, our RNAi screening identifies previously undescribed genes involved in mutant Htt aggregation in mammalian cells.

Results

Identification of shRNAs that modify mutant Nhtt aggregation in neuro2a cells

To identify modifiers of mutant Htt aggregation in mammalian cells, we performed shRNA screening using mouse neuro2a cells that inducibly expressed exon 1 of Htt (Nhtt) containing a 150Q tagged with an EGFP at its C-terminus (Nhtt150Q-EGFP), under the control of ponasterone A [35]. shRNA libraries were purchased from Open Biosystems, in which shRNA clones were supplied as *E. coli* glycerol stocks in 96 well plate-formats. We used total 122 plates for plasmid DNA purification and obtained 11346 shRNA clones with transfection grade DNA. Scheme of experimental procedure is outlined in Figure 1. First, neuro2a cells were seeded on 96 well plates and transiently transfected with shRNA clones. Cells were then differentiated by dibutyryl cyclic AMP (dcAMP) on the same day and selected with puromycin on the next day. After the selection, they were treated with ponasterone A to induce Nhtt150Q-EGFP expression. EGFP positive aggregates will be allowed to form for one day. After fixation and nuclear staining with DAPI or Hoechst, the number of aggregates-containing cells and total number of cells were automatically quantified by Cellomics ArrayScan HCS Reader, a cell image analyzer equipped with fluorescence microscopy.

The screening strategy is summarized in Figure 2. In the first screening, we screened 11346 shRNA clones based on the z score (mean z score is <-1.5 or >1.5) and finally obtained 602 shRNAs that were able to modify Nht150Q-EGFP aggregation in neuro2a cells (Figure 3A). To exclude the shRNAs that modify the aggregation purely acting on Nhtt expression itself, we performed a second screen, in which we used neuro2a cells expressing non-aggregating Nhtt16Q-EGFP [35]. After transfection and induction of Nhtt16Q-EGFP expression as above, EGFP intensities in the cells were quantified by ArrayScan reader. Through this analysis, we noticed that the shRNAs that induced Nhtt16Q-EGFP expression were relatively enriched in the aggregation-enhancing shRNAs (Figure 3B), suggesting that their enhancing effect was just caused by inducing Nhtt expression. After the second screen, 270 shRNAs were remained as candidates as they did not show significant alteration in Nhtt16Q-EGFP expression (Figure 3B). To obtain shRNAs that reproducibly modifying aggregation, we again used Nhtt150Q-EGFP cells for the third screening. Finally, we

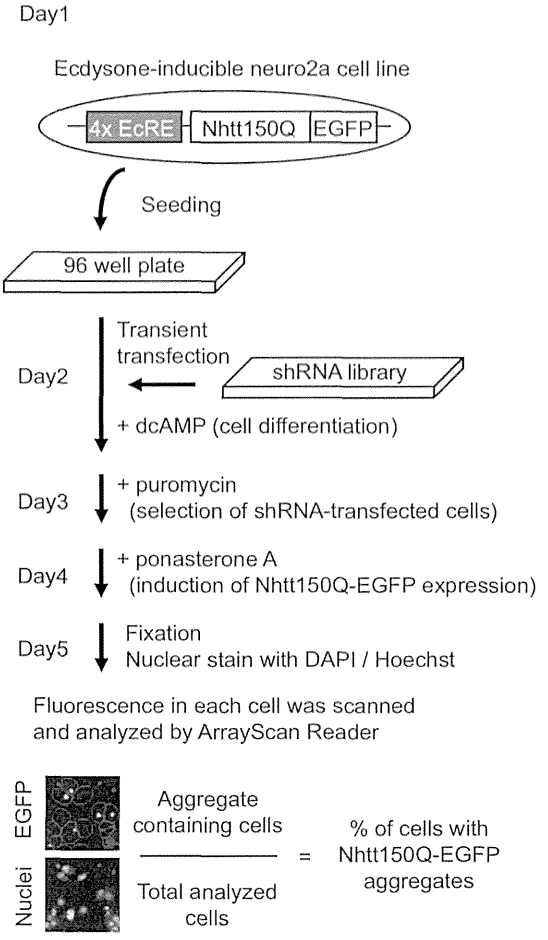

Figure 1. Experimental procedure of screening of shRNAs that modify Nhtt150Q-EGFP aggregation in neuro2a cells. Neuro2a cells inducibly expressing Nhtt150Q-EGFP under ecdysone-responsive element (EcRE) were seeded on a 96 well culture plate. On the next day, the cells were transiently transfected with shRNAs prepared from shRNA library plates. The cells were then differentiated by dcAMP on the same day and selected with puromycin on the next day, after which they were treated with ponasterone A to induce Nhtt150Q-EGFP expression. After 24 hr, the cells were fixed with 4% PFA and incubated with DAPI or Hoechst for nuclear staining. Fluorescence cell images were automatically obtained and analyzed by ArrayScan HCS Reader, and percent of cells with Nhtt150Q-EGFP aggregates among total analyzed cells was calculated.
doi:10.1371/journal.pone.0093891.g001

obtained 111 shRNAs that specifically and reproducibly modified Nhtt150Q-EGFP aggregation in neuro2a cells (Figure 3C).

Validation, classification and proteasome-dependency of the aggregation-modification by the identified shRNAs

Among the final 111 shRNAs, 63 suppressed and 48 enhanced the aggregation of mutant Nhtt (Table 1, 2) (complete screening data for 111 candidates are described in Data S1). Figure 3D shows representative cell images of the aggregation-modification by the shRNAs; Atf3 or Ppt2 shRNAs reduced Nhtt-150QEGFP aggregates compared with non-silencing control whereas Cish or Gnai2 shRNAs increased them. To validate the gene-knockdown effect by the shRNAs, we designed other RNAi sequences (Inv-1 and -2) by Invitrogen's BLOCK-iT RNAi Designer for some of the genes (Data S2), and expressed as miRNA (miR RNAi) using

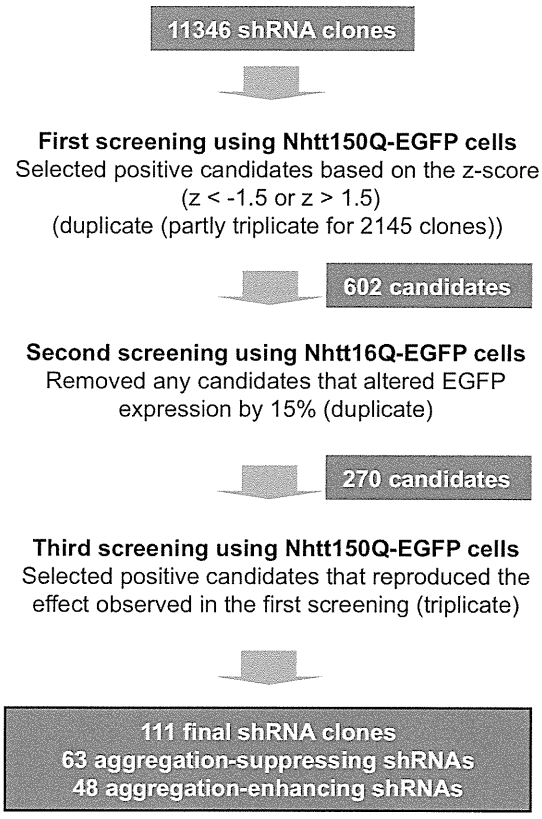

Figure 2. Summary of the shRNA screening. Total 11346 shRNA clones were subjected to the first screening using Nhtt150Q-EGFP cells. The screening was performed in duplicate (partly in triplicate), and shRNAs altering Nhtt150Q-EGFP aggregation at <-1.5 or >1.5 of z-score were selected as positive candidates. Obtained 602 clones were then subjected to the second screening using Nhtt16Q-EGFP cells to exclude the shRNAs modifying the aggregation by altering Nhtt expression itself. shRNAs altering EGFP intensity by 15% compared with the control were removed. Remaining 270 candidates were subjected to the third screening using Nhtt150Q-EGFP cells for confirmation (triplicate). We performed statistical analysis (t-test) in the third screening and shRNAs with $P<0.1$ were included as candidates. Finally, 111 shRNAs were obtained, among which 63 shRNAs suppressed and 48 shRNAs enhanced the Nhtt150Q-EGFP aggregation.
doi:10.1371/journal.pone.0093891.g002

pcDNA6.2-mRFP-miR vector [36]. We reproduced the aggregation-modifying ability in 12 out of 15 genes (80%) by at least one of the miRNAs (Figure 3E), supporting the validity of our screening strategy and results.

To examine the molecular mechanism underlying mutant Nhtt aggregation by these shRNAs, we classified the final 111 shRNA-target genes using PANTHER Classification System [37]. When focused on molecular function, they were classified into various functions such as catalytic, receptor and transcription regulator activities (Figure 4A). Classification by PANTHER protein class also suggests the genes with various activities involved in mutant Nhtt aggregation (Figure 4B). Another Classification method further suggests the involvement of multiple biological processes in the aggregation modification (Figure 4C). Although no marked difference was observed between the target genes of the aggregation-suppressing and -enhancing shRNAs, transcription factors such as Atf3 and Tcf20 was more abundant in the suppressors' targets (12.7%; 8 out of 63) than the enhancers' targets (4.1%; 2 out of 48) (Figure 4A, B). In contrast, genes for membrane trafficking such as Stxbp1 and Snx10 were only found in the enhancers' targets (8.3%; 4 out of 48) (Figure 4B). We also performed Statistical Overrepresentation Test using PANTHER Classification System, however any of gene ontology (GO) term or pathway was not significantly enriched (data not shown). These data suggest that genes with broad molecular and biological functions modify the mutant Nhtt aggregation whereas some specific cellular functions such as gene transcription and membrane trafficking may be differentially involved in the modification.

Several lines of studies have suggested an involvement of ubiquitin-proteasome system, a major protein degradation system in cells, in mutant Htt degradation [34,38–41]. In addition, another degradation system, autophagy, is also recently shown to be involved in clearance mutant Htt aggregates [36,42–45]. To examine whether the aggregation-modification by identified shRNAs involves these systems, we picked up 10 aggregation-suppressing shRNAs whose targets have various molecular and biological functions (Figure 4), and examined their effect in the presence of MG132 or bafilomycin A1 (Baf A1), inhibitor of proteasome or autophagy, respectively. We found that MG132 but not Baf A1 relieved the aggregation-suppressing effect of several shRNAs, such as those for Atf3, Cradd, Tmem179b and Pdcd4 (Figure 5), suggesting that these genes modify the mutant Nhtt aggregation through proteasome-dependent mechanism.

Tcf20 binds to mutant Nhtt aggregates in neuro2a cells and R6/2 mouse brain neurons

In addition to the genes whose shRNAs' effect was sensitive to MG132 as described above, we found several genes including Ppt2 and Tcf20 whose shRNAs' effect was insensitive to it (Figure 5), suggesting proteasome-independent modification by these genes. Among them, we focused on Tcf20 because it is relatively Q-rich (Q composition is 9.7%) among the identified modifiers (mean Q composition is $4.59\pm1.92\%$) and notably it contains several polyQ stretches in the N-terminal region (Figure 6A). Because some of Q-rich proteins are shown to directly co-aggregate with mutant Htt [3–6,8,9], it is possible that Tcf20 directly interacts with mutant Nhtt aggregates.

To examine this possibility, we cloned Tcf20 cDNA into pcDNA-DEST40 vector with a V5 tag at its C-terminus, and expressed Tcf20-V5 in neuro2a cells together with Nhtt150Q-EGFP-NLS (nuclear localization signal). As shown in Figure 6B, Tcf20-V5 was clearly co-localized with Nhtt150Q-EGFP-NLS aggregates, whereas it was only diffusely localized in the nucleus in the cells without the aggregates. Tcf20-V5 was also co-localized with cytoplasmic Nhtt150Q-EGFP aggregates (Figure 6C). In contrast, these co-localization was not observed for LacZ or other potential modifiers without polyQ-stretch such as Rab2b and Ddr2 (Q compositions are 5.6% and 4.0%, respectively) (Figure 6C; Ddr2, data not shown). We further found that Tcf20 N-terminal constructs (1~400 and 1~500) containing polyQ stretches preferentially co-localized with Nhtt150Q-EGFP aggregates (Figure 6C). In addition, these were insolubilized with Nhtt150Q-EGFP but not with Nhtt16Q-EGFP (Figure 6D), similar to a known aggregates-interacting protein, NF-YA [5]. Interestingly, overexpression of either N-terminal (1~400 and 1~500) or full-length of Tcf20 suppressed Nhtt150Q-EGFP aggregation (Figure 6E), suggesting that the Tcf20 interaction through its N-terminus suppresses mutant Nhtt aggregation when overexpressed. Finally, an antibody against Tcf20 stained puncta positive for Htt and Ub in cortical neurons of HD model mouse (Figure 7A, B), suggesting *in vivo* incorporation of Tcf20 into

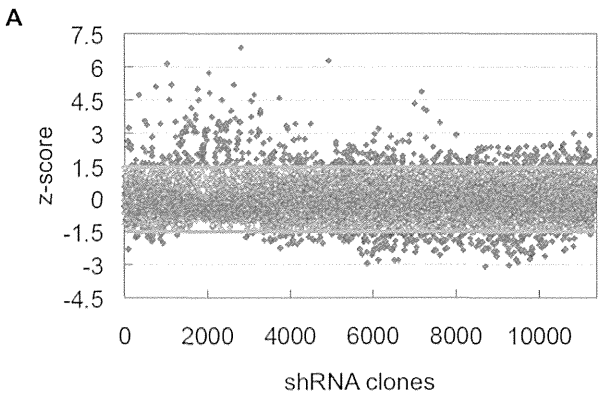

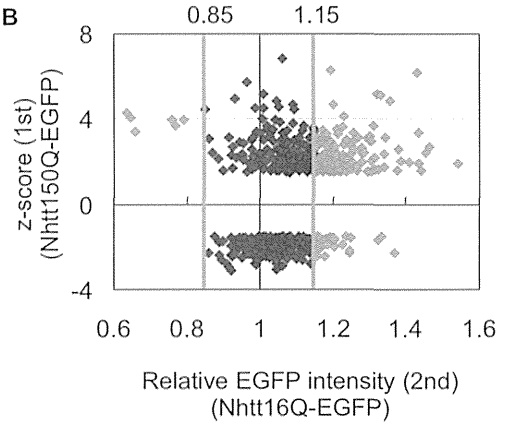

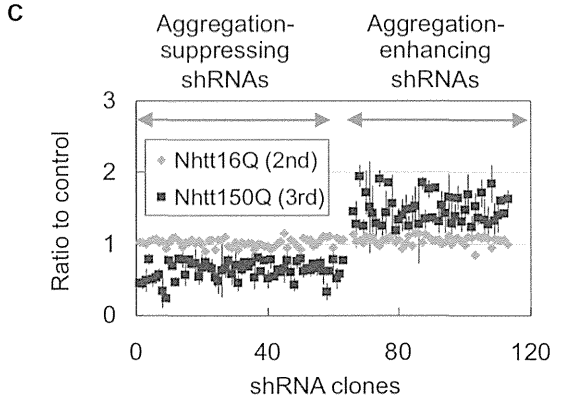

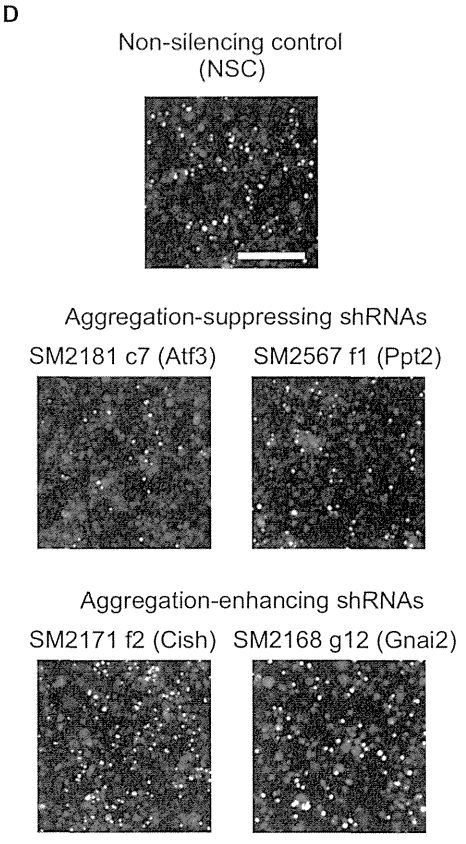

E

Gene	OBS shRNA Clone ID		Invitrogen miRNA Inv-1	Inv-2
Ddr2	SM2185 h3	S	S	S
Fbxw8	SM2588 a1	S	S	S
Ppt2	SM2567 f1	S	S	S
Pik3c2a	SM2185 g9	S	S	S
	SM2183 c12	S		
Atf3	SM2181 c7	S	S	N
Rab2b	SM2593 c6	S	S	E
Tcf20	SM2181 e5	S	S	N
Csnk1d	SM2186 h9	S	S	N
Gnpda1	SM2575 d8	E	E	N
Map3k1	SM2187 d12	E	E	N
Nap1l4	SM2169 g11	S	S	E
Pip5k1b	SM2185 f10	E	E	S
Cradd	SM2176 a9	S	N	E
Tmem179b	SM2175 d6	S	N	E
Pdcd4	SM2176 d1	S	N	N

Figure 3. Identification and validation of the shRNAs modifying Nhtt150Q-EGFP aggregation in neuro2a cells. (A) Summarized data of the first screening using Nhtt150Q-EGFP cells. Mean z-score of 11346 shRNA clones were plotted. shRNAs showing the z-score outside the range of ±1.5 were picked up as positive candidates (indicated as blue plots). (B) Summarized data of the second screening using Nhtt16Q-EGFP cells. The data (relative EGFP intensity; x-axis) were plotted against the first screening data (z-score; y-axis) for 602 shRNA clones. The shRNAs showing the EGFP intensity within 15% to the control were picked up as positive candidates (indicated as blue plots). (C) Data of the second and third screening for final 111 shRNA candidates. 63 shRNAs suppressed and 48 shRNAs enhanced the Nhtt150Q-EGFP aggregation without distinct alteration of Nhtt16Q-EGFP expression. (D) Example cell images. Two shRNAs targeting Atf3 or Ppt2 reduced the cells with Nhtt150Q-EGFP aggregates compared with non-silencing control whereas two shRNAs targeting Cish or Gnaj2 increased them. Bar is 0.2 mm. (E) Validation of the effect of Open Biosystems (OBS) shRNA by two miRNAs (Inv-1 and -2) binding to different sequences of the genes (Data S2). The S, N and E mean suppression, no-effect and enhancement for the Nhtt150Q-EGFP aggregation, respectively. In case of Pik3c2a, two different shRNAs were obtained. Note that the shRNA's effect was reproduced by at least one miRNA in 12 genes (80% of analyzed genes).
doi:10.1371/journal.pone.0093891.g003

inclusions containing mutant Nhtt aggregates. These data suggest that the Tcf20 specifically interacts with mutant Nhtt aggregates through its N-terminus containing polyQ stretches to be incorporated into the inclusion. Because both knockdown and overexpression showed suppressive effect on mutant Nhtt aggregation, moderate expression of Tcf20 might be appropriate for efficient aggregation. Alternatively, its direct interaction and transcriptional activity could be differentially involved in the regulation of mutant Nhtt aggregation.

Table 1. shRNAs suppressing Nhtt150Q aggregation in neuro2a cells.

	shRNA		1st (150Q)	2nd (16Q)	3rd (150Q)	
No	Clone ID	Gene	z-score	Ratio	Ratio (+ SD)	Gene Description
1	SM2173 d5	1810032O08Rik	−1.79	1.03	0.447 (+0.084)	RIKEN cDNA 1810032O08 gene
2	SM2177 c4	4933425L06Rik	−2.17	1.02	0.447 (+0.160)	RIKEN cDNA 4933425L06 gene
3	SM2179 b7	Abat	−1.65	0.99	0.493 (+0.086)	4-aminobutyrate aminotransferase
4	SM2574 c8	Aktip	−1.60	1.03	0.787 (+0.090)	thymoma viral proto-oncogene 1 interacting protein
5	SM2181 c7	Atf3	−1.51	1.06	0.499 (+0.093)	activating transcription factor 3
6	SM2172 b5	Birc6	−2.29	1.07	0.533 (+0.098)	baculoviral IAP repeat-containing 6
7	SM2173 f4	Casp3	−1.52	1.02	0.563 (+0.237)	caspase 3
8	SM2174 e3	Cd24a	−2.45	1.03	0.339 (+0.066)	CD24a antigen
9	SM2176 a9	Cradd	−2.27	0.93	0.241 (+0.028)	death domain-containing protein, RAIDD
10	SM2186 h9	Csnk1d	−2.22	1.03	0.771 (+0.060)	casein kinase 1, delta
11	SM2185 h3	Ddr2	−1.52	1.09	0.699 (+0.069)	discoidin domain receptor family, member 2
12	SM2168 c8	Ddx6	−1.75	1.10	0.467 (+0.038)	DEAD (Asp-Glu-Ala-Asp) box polypeptide 6
13	SM2579 f9	Efhb	−2.60	1.05	0.793 (+0.122)	EF hand domain family, member B
14	SM2558 e11	Enah	−1.55	0.96	0.787 (+0.148)	enabled homolog (Drosophila)
15	SM2588 a1	Fbxw8	−1.57	1.03	0.564 (+0.056)	F-box and WD-40 domain protein 8
16	SM2561 e3	Fcgr3	−1.90	1.02	0.781 (+0.024)	Fc receptor, IgG, low affinity III
17	SM2176 h8	Fgd1	−1.92	1.06	0.719 (+0.200)	FYVE, RhoGEF and PH domain containing 1
18	SM2560 h6	Fkbp9	−2.34	1.01	0.736 (+0.117)	FK506 binding protein 9
19	SM2179 b5	Fsd1l	−1.62	1.04	0.548 (+0.199)	FSD1-like
20	SM2179 e8	Gaa	−2.25	0.99	0.664 (+0.095)	glucosidase, alpha, acid
21	SM2560 e6	Gjb2	−1.77	0.89	0.743 (+0.036)	gap junction protein, beta 2
22	SM2177 e1	Gpr37	−2.79	1.05	0.680 (+0.141)	G protein-coupled receptor 37
23	SM2588 f3	Grhpr	−2.14	1.07	0.654 (+0.129)	glyoxylate reductase/hydroxypyruvate reductase
24	SM2174 g6	Hoxd3	−1.96	0.92	0.527 (+0.167)	homeobox D3
25	SM2175 c6	Jagn1	−1.68	1.06	0.473 (+0.381)	jagunal homolog 1 (Drosophila)
26	SM2591 e6	Klhl7	−1.66	1.06	0.635 (+0.120)	kelch-like 7
27	SM2134 h10	LOC195242	−1.92	1.10	0.650 (+0.099)	
28	SM2112 g12	LOC195373	−1.59	0.98	0.763 (+0.150)	
29	SM2185 a7	Lrguk	−1.79	0.95	0.577 (+0.211)	leucine-rich repeats and GUK containing
30	SM2587 b3	Mab21l3	−1.67	1.03	0.702 (+0.115)	mab-21-like 3 (C. elegans)
31	SM2169 g11	Nap1l4	−1.57	0.92	0.455 (+0.072)	nucleosome assembly protein 1-like 4
32	SM2146 b6	Nlrp10	−1.54	1.02	0.641 (+0.058)	NLR family, pyrin domain containing 10
33	SM2575 b10	Notch4	−2.02	1.00	0.745 (+0.048)	notch 4
34	SM2176 f1	Olfr1339	−1.99	1.01	0.676 (+0.118)	olfactory receptor 1339
35	SM2008 a5	Olfr1451	−1.94	1.01	0.746 (+0.160)	olfactory receptor 1451
36	SM2174 c1	Olfr339	−2.96	0.92	0.526 (+0.062)	olfactory receptor 339
37	SM2142 b5	Olfr530	−1.89	0.99	0.808 (+0.042)	olfactory receptor 530
38	SM2588 f4	Olfr668	−2.65	1.00	0.623 (+0.049)	olfactory receptor 668
39	SM2562 d2	P2ry1	−1.94	0.97	0.764 (+0.136)	purinergic receptor P2Y, G-protein coupled 1
40	SM2176 d1	Pdcd4	−2.32	0.97	0.512 (+0.123)	programmed cell death 4
41	SM2575 a6	Pf4	−2.46	0.93	0.780 (+0.041)	platelet factor 4
42	SM2183 c12	Pik3c2a	−2.08	0.96	0.548 (+0.057)	PI 3-kinase, C2 domain containing, alpha
43	SM2185 g9	Pik3c2a	−1.99	1.01	0.637 (+0.043)	PI 3-kinase, C2 domain containing, alpha
44	SM2134 a11	Pkd1l3	−1.53	1.03	0.606 (+0.198)	polycystic kidney disease 1 like 3
45	SM2177 e5	Plec	−1.82	1.15	0.657 (+0.134)	plectin
46	SM2148 a11	Ppfia1	−1.58	0.95	0.775 (+0.107)	PTPRF, interacting protein (liprin), alpha 1
47	SM2567 f1	Ppt2	−2.15	1.06	0.605 (+0.093)	palmitoyl-protein thioesterase 2
48	SM2149 a9	Ptprn2	−2.03	1.02	0.434 (+0.103)	protein tyrosine phosphatase, receptor type, N2

Table 1. Cont.

No	shRNA Clone ID	Gene	1st (150Q) z-score	2nd (16Q) Ratio	3rd (150Q) Ratio (+ SD)	Gene Description
49	SM2593 c6	Rab2b	−2.36	0.97	0.754 (+0.076)	RAB2B, member RAS oncogene family
50	SM2567 a8	Racgap1	−2.34	0.93	0.789 (+0.079)	Rac GTPase-activating protein 1
51	SM2008 h8	Rfc1	−1.65	1.09	0.614 (+0.074)	replication factor C (activator 1) 1
52	SM2588 d5	Rps27l	−1.58	1.06	0.660 (+0.087)	ribosomal protein S27-like
53	SM2169 b7	Slc25a14	−1.96	1.07	0.630 (+0.039)	solute carrier family 25member 14
54	SM2558 f9	Stfa3	−1.99	0.97	0.717 (+0.104)	stefin A3
55	SM2591 c7	Taf7l	−1.64	0.99	0.659 (+0.101)	TAF7-like RNA polymerase II, TBP-associated factor
56	SM2573 d3	Tbx18	−2.25	1.07	0.733 (+0.184)	T-box18
57	SM2181 e5	Tcf20	−1.94	1.11	0.613 (+0.114)	transcription factor 20
58	SM2175 d6	Tmem179b	−2.57	1.10	0.334 (+0.055)	transmembrane protein 179B
59	SM2591 c1	Tmem25	−1.61	1.11	0.620 (+0.099)	transmembrane protein 25
60	SM2141 e9	Trappc9	−1.62	0.95	0.778 (+0.149)	trafficking protein particle complex 9
61	SM2587 g7	Tspan10	−2.22	1.09	0.514 (+0.035)	tetraspanin 10
62	SM2149 a4	Txlna	−1.78	1.06	0.579 (+0.021)	taxilin alpha
63	SM2579 c2	Wdr37	−1.92	1.06	0.764 (+0.122)	WD repeat domain 37

List of 63 shRNAs suppressing Nhtt150Q-EGFP aggregation without distinct alteration of Nhtt16Q-EGFP expression in neuro2a cells. Targets genes of shRNAs and data summary of 1st (z-score), 2nd (ratio to control) and 3rd screening (ratio to control ± SD) are described. In case of Pik3c2a, two different shRNAs were obtained. Clone IDs of shRNAs are originally named in this paper based on plate number and well position of the shRNA.

doi:10.1371/journal.pone.0093891.t001

We have previously performed mass spectrometry of Nhtt150Q-EGFP aggregates purified from neuro2a cells and identified several aggregate-interacting proteins such as ubiquilin-1,-2, FUS/TLS and NF-YA/-YC [5,8,46]. By re-checking the data, we noticed that Tcf20 was contained in the mass spectrometry data. In addition, we found other modifiers, Hdac5 and Arhgap24, in the data, suggesting they are also the proteins incorporated into the aggregates. Analysis of their amino acid sequences revealed that Hdac5 but not Arhgap24 is relatively Q-rich (Q compositions are 8.9% and 4.8%, respectively). We also analyzed the Q composition of rest of the modifiers, however protein significantly in Q-rich like Tcf20 or Hdac5 was not found (data not shown). Taken together, these data suggest that Tcf20 and potentially Hdac5 are the proteins directly interacting with mutant Nhtt aggregates among the identified aggregation-modifiers.

Suppression of mutant Nhtt aggregation by knocking down of Csnk1d and Pik3c2a

To identify other molecular mechanisms regulating mutant Nhtt aggregation, we focused on kinases, key regulators of intracellular signal transduction. Our screening identified several kinases as potential modifiers for mutant Nhtt aggregation (Table 1, 2). These include Csnk1d, Pik3c2a and Lrguk, whose shRNAs suppressed the aggregation, and Cmpk1, Map3k1 and Pip5k1b, whose shRNAs enhanced it. The aggregation-modifying effect of these shRNAs can be reproduced when we used our own miRNAs that bind to same region as shRNA (OBS miRNA; Figure 8A), or different region (Inv-1 or -2 miRNA; Figure 1E, 8B) supporting the validity of gene knockdown effect of these kinases on the aggregation-modification. We then focused on two kinases, Csnk1d and Pik3c2a, whose knockdown suppressed Nhtt150Q-EGFP aggregation, and confirmed significant and specific reduction of gene expressions by their miRNAs (Figure 8C). We further examined the dependency of their knockdown effect on proteasome or autophagic activity, and found that their miRNAs were still effective even in the presence MG132 or Baf A1 (Figure 8D). Taken together, these data suggest that Csnk1d and Pik3c2a are involved in the modification of mutant Nhtt aggregation through proteasome- and autophagy-independent mechanisms.

Knockdown of aggregation-modifiers did not suppress mutant Nhtt-induced cell toxicity

Finally, we examined the effect of knockdown of Tcf20, Csnk1d or Pik3c2a on cell toxicity induced by mutant Nhtt. For this purpose, we first synthesized following siRNA oligos based on the miRNA sequences used above; two for Tcf20 (OBS and Inv-1) and one for Csnk1d (Inv-1) or Pik3c2a (Inv-1). We first confirmed that transduction of these siRNA induced significant and specific reduction of their target genes compared with that of non-targeting control (NT) in neuro2a cells (Figure 9A). We then transiently overexpressed Nhtt16Q-EGFP or Nhtt150Q-EGFP in siRNA-transduced cells. After two days, the cells were incubated with pyridinium iodide (PI) to detect dead cells, and percent of PI-positive cells per GFP-positive, Nhtt expressing cells was calculated by ArrayScan. As shown in Figure 9B, overexpression of Nhtt150Q-EGFP induced ~3-fold increase in PI-positive cells compared with that of Nhtt16Q-EGFP, suggesting the induction of cell toxicity by mutant Nhtt in neuro2a cells. Notably, knockdown of Tcf20, Csnk1d or Pik3c2a did not suppress the toxicity rather enhanced it, although their knockdown seemed to be also effective, but to a lesser extent, in Nhtt16Q-EGFP-expressing cells (Figure 9B). Altogether, these data suggest that downregulation of these modifiers dose not suppress mutant Nhtt toxicity in neuro2a cells.

Discussion

In this paper, we first performed large-scale shRNA screening of modifiers for mutant Htt aggregation in mammalian cells. By

Table 2. shRNAs enhancing Nhtt150Q aggregation in neuro2a cells.

No	Clone ID	Gene	1st (150Q) z-score	2nd (16Q) Ratio	3rd (150Q) Ratio (+ SD)	Gene Description
1	SM2592 c7	Aimp2	2.24	1.13	1.446 (+0.331)	ARS interacting multifunctional protein 2
2	SM2023 a1	Aldh3b1	2.98	1.04	1.270 (+0.158)	aldehyde dehydrogenase 3 family, member B1
3	SM2598 f6	Arhgap24	1.57	1.05	1.945 (+0.103)	Rho GTPase activating protein 24
4	SM2108 a4	C1qtnf9	5.15	1.01	1.246 (+0.311)	C1q and tumor necrosis factor related protein 9
5	SM2171 f2	Cish	2.20	1.11	1.717 (+0.647)	cytokine inducible SH2-containing protein
6	SM2563 h3	Clec4e	1.86	1.07	1.512 (+0.387)	C-type lectin domain family 4, member e
7	SM2566 f12	Cml1	1.71	1.10	1.427 (+0.170)	camello-like 1
8	SM2022 g1	Cmpk1	1.89	1.01	1.283 (+0.120)	cytidine monophosphate (UMP-CMP) kinase 1
9	SM2179 c5	Cnih2	1.63	0.98	1.905 (+0.244)	cornichon homolog 2 (Drosophila)
10	SM2570 c11	Gba	1.88	1.04	1.242 (+0.297)	glucosidase, beta, acid
11	SM2110 c2	Gm10336	2.09	1.07	1.439 (+0.055)	predicted gene 10336
12	SM2168 g12	Gnai2	2.18	1.07	1.855 (+0.408)	G protein alpha inhibiting 2
13	SM2575 d8	Gnpda1	1.74	1.14	1.559 (+0.104)	glucosamine-6-phosphate deaminase 1
14	SM2014 g8	Hdac5	3.51	1.02	1.182 (+0.162)	histone deacetylase 5
15	SM2598 a11	Krcc1	2.22	1.06	1.340 (+0.225)	lysine-rich coiled-coil 1
16	SM2021 a4	Lmln	4.98	0.93	1.398 (+0.218)	leishmanolysin-like (metallopeptidase M8 family)
17	SM2111 e11	LOC210191	2.06	1.01	1.476 (+0.136)	
18	SM2113 d11	LOC226712	2.83	1.11	1.250 (+0.188)	
19	SM2187 d12	Map3k1	1.67	0.98	1.491 (+0.280)	mitogen-activated protein kinase kinase kinase 1
20	SM2173 a12	Mark3	1.52	1.15	1.524 (+0.554)	MAP/microtubule affinity-regulating kinase 3
21	SM2577 h12	Mei1	1.97	1.15	1.278 (+0.093)	meiosis defective 1
22	SM2561 g8	Myl12b	3.45	1.03	1.850 (+0.131)	myosin, light chain 12B, regulatory
23	SM2576 e12	Myo19	1.57	1.13	1.345 (+0.124)	myosin XIX
24	SM2580 c2	Mypop	1.99	1.10	1.768 (+0.066)	Myb-related transcription factor, partner of profilin
25	SM2563 f11	P2rx7	1.60	1.05	1.357 (+0.036)	purinergic receptor P2X, ligand-gated ion channel, 7
26	SM2583 c6	Pcdhb18	1.58	1.05	1.776 (+0.165)	protocadherin beta 18
27	SM2593 d2	Pcgf3	2.47	1.06	1.307 (+0.198)	polycomb group ring finger 3
28	SM2561 h8	Pcp2	2.13	1.00	1.539 (+0.278)	Purkinje cell protein 2 (L7)
29	SM2185 f10	Pip5k1b	2.02	1.02	1.423 (+0.324)	phosphatidylinositol-4-phosphate 5-kinase, type 1 beta
30	SM2563 h5	Plp2	1.84	1.11	1.652 (+0.352)	proteolipid protein 2
31	SM2022 g10	Ptpn11	2.42	1.00	1.292 (+0.176)	protein tyrosine phosphatase, non-receptor type 11
32	SM2109 c7	Rassf4	3.49	1.08	1.382 (+0.167)	Ras association domain family member 4
33	SM2139 h11	Rnf20	2.06	1.09	1.644 (+0.143)	ring finger protein 20
34	SM2109 e10	Serpinb10	3.50	1.04	1.315 (+0.178)	serine peptidase inhibitor, clade B, member 10
35	SM2598 h10	Slain2	2.25	0.98	1.479 (+0.284)	SLAIN motif family, member 2
36	SM2583 c9	Snx10	1.83	1.10	1.691 (+0.168)	sorting nexin 10
37	SM2568 e11	Spa17	1.86	1.09	1.233 (+0.191)	sperm autoantigenic protein 17
38	SM2112 g7	Spata21	4.45	0.85	1.523 (+0.099)	spermatogenesis associated 21
39	SM2568 h10	St6galnac2	1.65	1.11	1.359 (+0.195)	ST6-N-acetylgalactosaminide alpha-2,6-sialyltransferase 2
40	SM2168 f8	Stxbp1	1.52	1.08	1.713 (+0.303)	syntaxin binding protein 1
41	SM2568 d8	Sult2a2	1.59	1.11	1.338 (+0.253)	sulfotransferase family 2A
42	SM2565 c8	Svep1	2.88	1.08	1.274 (+0.266)	sushi, EGF and pentraxin domain containing 1
43	SM2184 a10	Syk	2.91	0.95	1.844 (+0.251)	spleen tyrosine kinase
44	SM2559 f11	Syt10	1.74	1.07	1.322 (+0.248)	synaptotagmin X
45	SM2142 g10	Tbc1d10c	3.38	1.07	1.402 (+0.046)	TBC1 domain family, member 10c
46	SM2587 a10	Tmem63a	1.71	1.05	1.604 (+0.054)	transmembrane protein 63a
47	SM2565 b8	Trem1	1.95	1.06	1.419 (+0.125)	triggering receptor expressed on myeloid cells 1

Table 2. Cont.

No	Clone ID	Gene	1st (150Q) z-score	2nd (16Q) Ratio	3rd (150Q) Ratio (+ SD)	Gene Description
48	SM2583 e7	Wdpcp	2.38	1.00	1.627 (+0.187)	WD repeat containing planar cell polarity effector

List of 48 shRNAs enhancing Nhtt150Q-EGFP aggregation without distinct alteration of Nhtt16Q-EGFP expression in neuro2a cells. Targets genes of shRNAs and data summary of 1st (z-score), 2nd (ratio to control) and 3rd screening (ratio to control ± SD) are described. Clone IDs of shRNAs are originally named in this paper based on plate number and well position of the shRNA.
doi:10.1371/journal.pone.0093891.t002

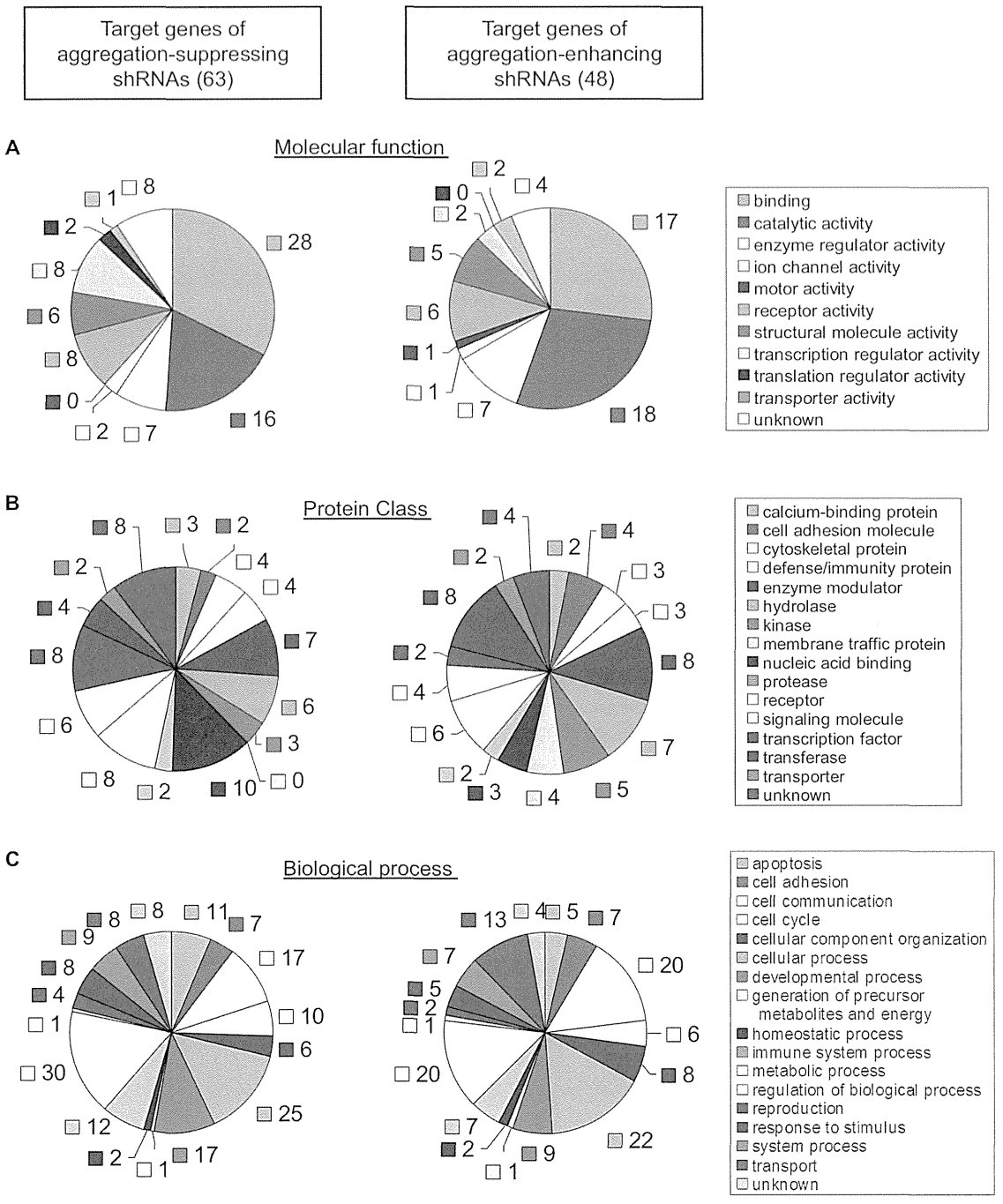

Figure 4. Classification of the shRNA-target genes. Target genes of the aggregation-suppressing (left chart) or -enhancing (right chart) shRNAs were classified using PANTHER Classification System based on molecular function (A), PANTHER Protein Class (B), or biological process (C). Genes not found in the database were classified as unknown. The numbers of classified genes were described.
doi:10.1371/journal.pone.0093891.g004

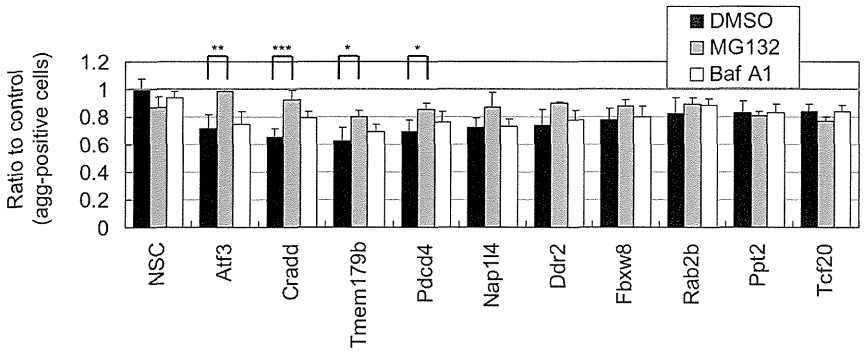

Figure 5. Effect of proteasome or autophagy inhibitor on shRNA-mediated modification of Nhtt150Q-EGFP aggregation. Nhtt150Q-EGFP cells transfected with control (NSC) or shRNAs for indicated genes were treated with 0.5 μM MG132, 0.5 μM Baf A1 or DMSO together with ponasterone A for 24 hr. The cells with Nhtt150Q-EGFP aggregates were quantified by ArrayScan reader. Some of shRNA's suppressive effects on the aggregation were relieved by treatment with MG132 but not with Baf A1. Values are means ± SD of four well data (*$P<0.05$, **$P<0.01$, ***$P<0.001$).
doi:10.1371/journal.pone.0093891.g005

transfection of neuro2a cell line expressing Nhtt with shRNA library clones and automated cell image analysis using ArrayScan HCS reader, we identified 111 shRNAs clones that specifically modified mutant Nhtt aggregation without affecting its expression in neuro2a cells. The shRNA-target genes were classified into various cellular functions including transcription and protein phosphorylation. Subsequent analysis suggests that in addition to the genes such as Atf3 whose knockdown effect was sensitive to proteasome inhibition, there were several genes whose knockdown modified the aggregation independently of it (Figure 10). These include a transcription factor Tcf20 and kinases Csnk1d and Pik3c2a. Notably, all the genes except Pik3c2a [33] are not found by the previous screenings using other organisms such as *Drosophila* and *C. elegans*. Thus, our RNAi screening using mammalian cells identified novel genes that modify mutant Htt aggregation through several, possibly mammalian-specific molecular mechanisms.

An identified modifier, Tcf20 (transcription factor 20), contains several polyQ stretches. Notably, Tcf20, as well as another relatively Q-rich modifier Hdac5 (histone deacetylase 5), was found in mutant Htt aggregates by our previous mass spectrometric analysis [46]. Indeed, we found co-localization and co-insolubilization of Tcf20 with mutant Nhtt aggregates through its N-terminal Q-rich region. In addition, anti-Tcf20 antibody stained nuclear inclusions of R6/2 mouse brain. Furthermore, overexpression of Tcf20 also modified the aggregation. These observations support the idea of physical and probably direct interaction of Tc20 with mutant Htt aggregates, which modifies the aggregation. We have previously shown that an RNA binding protein FUS/TLS, another protein identified by the mass spectrometry described above, suppresses mutant Htt aggregation [8]. In contrast, GIT1 (G protein-coupled receptor kinase-interacting protein), identified by a yeast two-hybrid screen using mutant Htt as a bait, enhances its aggregation [47]. These observations suggest that mutant Htt aggregation is differentially modulated by several interacting proteins, and Tcf20 or Hdac5 may also be the protein that directly modifies it (Figure 10). Interestingly, the modifiers identified here also include several aggregation-prone proteins such as Cradd/Raidd [48], Gpr37/Pael-R [49] and Aimp2/p38 [50]. It would be intriguing to test the co-aggregation of these with mutant Htt, which could lead to identification of another potential mechanism of direct modification of the mutant Htt aggregation.

We also found several kinases that modify the mutant Htt aggregation. One of them is Csnk1d (casein kinase 1 delta; CK1δ), a CK1 family kinase that phoshorylates many substrates with different cellular functions such as cell differentiation, proliferation, chromosome segregation and circadian rhythm [51]. Pathologically, CK1 is shown to be elevated in Alzheimer patients, and phosphorylate tau, a protein linked to Alzheimer's diseases [51]. Although the role of CK1 in polyQ diseases is unknown, overexpression of another casein kinase, CK2, is shown to reduce mutant Htt aggregates possibly through p62-madiated autophagic clearance [36]. Because we found that Csnk1d knockdown reduces the aggregates, mutant Htt aggregation may be differentially modified through these two casein kiasnes, CK1 and CK2 (Figure 10).

Another identified modifier, Pik3c2a (phosphatidylinositol 3 kinase C2 alpha; PI3K-C2α), is a class II PI3K that phosphorylates 3′ position of inositol lipids to produce mainly phosphatidylinositol 3-phosphate (PI(3)P) [52,53]. Because Pik3c2a knockdown is also shown to reduce mutant Htt aggregation in *Drosophila*, it is an evolutionally conserved modifier of the aggregation. When compared with class I conventional PI3K that produces mainly $PI(3,4,5)P_3$ [52], Pik3c2a has unique structural features, including a clathrin-binding site in the N-terminal stretch, and relative resistance to PI3K inhibitors wortmannin and LY294002 [52,54]. Although recent studies suggest its involvement in intracellular vesicular trafficking and tissue morphogenesis [54–57], the mechanism by which Pik3c2a modifies mutant Htt aggregation remains unknown. One potential pathway is through regulation of RhoA small GTPase, because Pik3c2a knockdown impaired RhoA activation in endothelial cell [57], and an inhibitor of Rho kinase, a downstream target of RhoA, suppresses mutant Htt aggregation in neuro2a cells [58]. In contrast, we found that mutant Htt aggregation was enhanced by knocking down another PI kinase, Pip5k1b, which phosphorylates 5′ position of inositol lipids to produce $PI(4,5)P_2$. Increased aggregation of mutant Htt has been also reported by suppression of a class III PI3K, Vps34, a key regulator of autophagic clearance of mutant Htt [45]. Thus, several phosphatidylinositols produced by different PI kinases may differentially modulate mutant Htt aggregation possibly through multiple molecular pathways (Figure 10).

Despite the suppression of mutant Nhtt aggregation by knocking down Tcf20, Csnk1d or Pik3c2a, we could not observe clear alteration of mutant Nhtt-induced cell toxicity by it. One possibility is that downregulation of only one gene is insufficient to alter the toxicity. Indeed, functional and/or physical interaction with polyglutamine proteins are also reported for several other shRNA target genes, such as Atf3 [59], Ddx6 [60], Fbxw8 [61], P2ry1 [62] and Map3k1 [63]. In addition, several shRNA targets

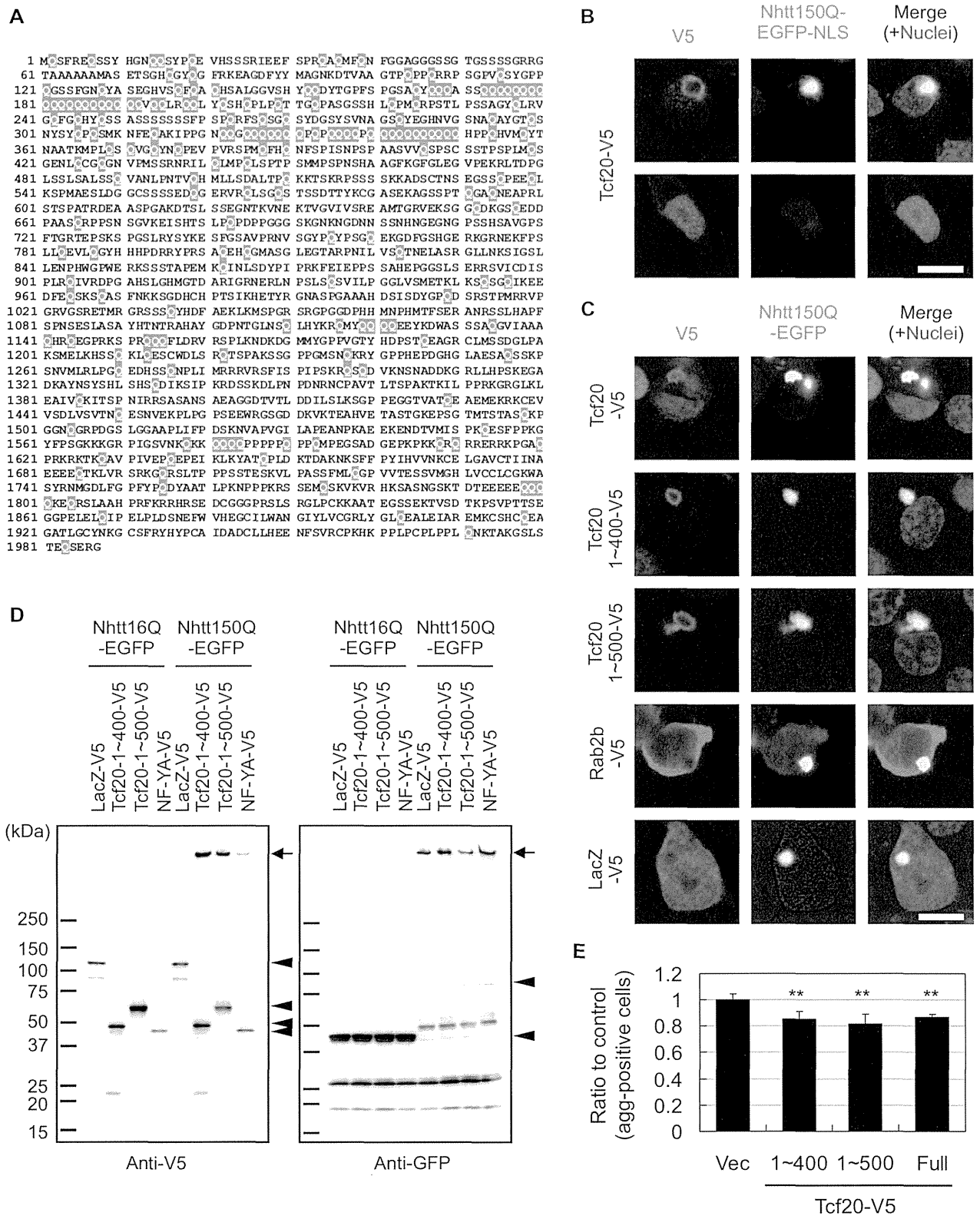

Figure 6. Tcf20 interacts with mutant Nhtt aggregates through its N-terminal region in neuro2a cells. (A) Primary sequences of mouse Tcf20. Glutamine (Q) residues were marked by red. Note that several polyQ stretches are observed in its N-terminal region. (B, C) Neuro2a cells were transfected with expression vectors for Nhtt150Q-EGFP-NLS (B) or Nhtt150Q-EGFP (C) together with those for indicated V5-tagged proteins. After one day, the cells were fixed and stained with anti-V5 antibody and Alexa 546-conjugated anti-mouse IgG. Nuclei were stained with DAPI. (B) Tcf20 co-accumulated with Nhtt150Q-EGFP-NLS aggregate in nucleus whereas it diffusely located in the nucleus without the aggregate. (C) Tcf20 or its N-terminal fragments accumulated with Nhtt150Q-EGFP aggregates in cytoplasm whereas Rab2b or LacZ did not. (D) Neuro2a cells were co-transfected with Nhtt150Q-EGFP expression vectors together with those for indicated V5-tagged proteins. After one day, the cells were subjected to Western blot